2017

A numerical investigation of cavitation in valves and techno-economic analysis of Pinewood solvent liquefaction

Daudet Nsabengo Nzombo
Iowa State University

A numerical investigation of cavitation in valves and techno-economic analysis of Pinewood solvent liquefaction

by

Daudet Nzombo

A thesis submitted to the graduate faculty

in partial fulfillment of the requirements for the degree of

MASTER OF SCIENCE

Major: Mechanical Engineering

Program of Study Committee:
Mark Mba-Wright, Major Professor
Theodore Heindel
Yu Wang

The student author and the program of study committee are solely responsible for the content of this thesis. The Graduate College will ensure this thesis is globally accessible and will not permit alterations after a degree is conferred.

Iowa State University

Ames, Iowa

2017

DEDICATION

I would like to dedicate this thesis to the memory of my late mother, Clementine Wanga, who I dearly miss, and whose advice and unconditional love help me thrive in life.

TABLE OF CONTENTS

LIST OF FIGURES

Page

LIST OF TABLES

NOMENCLATURE

AF	Atomic mass fraction
CAPEX	Capital Expenditure
CFD	Computational Fluid Dynamics
CHP	Combined Heat and Power
CV	Control Volume
D	Pipe Diameter
DCFROR	Discounted Cash Flow Rate of Return
DDB	Double Declining Balance
DIC	Direct Installed Cost
DOE	Design of Experiment
$\vec{F}$	Body force
FCI	Fixed Capital Investment
FCV	Finite Control Volume
GHG	Greenhouse Gases
HLCO	Hydrogenated Light Cycle Oil
SL	Hydrothermal Liquefaction
HWO	Heavy Wood Oil
IRR	Internal Rate of Revenue
LA	Light Acids
LWO	Light Wood Oil
MF	Mass fraction
MFSP	Minimum Fuel Selling Price

MOGA	Multiple-Objective Optimization Method
MW	Mega Watt
MWO	Medium Wood Oil
NCG	Non-Condensable Gases
OPEX	Operating Expenditure
P	Phenols
P	Local static pressure
P_v	Vapor pressure
R_B	Bubble radius
R_e, R_c	Mass transfer between the liquid and vapor phases in cavitation
RSO	Response Surface Optimization
TEA	Techno-Economic Analysis
TIC	Total Installed Cost
TPEC	Total Purchased Equipment Cost
TPI	Total Project Investment
$\overrightarrow{V_m}$	Local Mass-averaged Velocity
U	Undetermined
W	Water

Subscripts

e	Evaporation
k	Phase K
l	Liquid phase
m	Mixture
v	Vapor phase

Symbols

α	Vapor volume fraction
ρ	Density
μ	Dynamic viscosity

ACKNOWLEDGMENTS

First and foremost, I would thank and express my gratitude to my major professor Mark Mba-Wright. His kindness, patience, support, and help during my master program. I would also like to thank my committee members Dr. Heindel and Dr. Wang for devoting their valuable time to serve as committee members.

Second, I would like to thank my friends and colleagues in BRT and ME for all their supports. I would also like to thank my parents, specially my father, Simon Nzombo, who deeply invested in my education, and have always encouraged me in furthering my education.

Third, I would also like to thank my mother in law, for watching my beautiful children while I spent countless hours at the library.

Last, but not least, I would like to thank my wife, Patience Nzombo, for her endless love, support, and encouragement. I'm truly and deeply grateful for all the sacrifices you have made.

CHAPTER 1. GENERAL INTRODUCTION

Motivation

Valves are devices used in the industry to control the flow by varying the size of the flow passage manually or when a signal is sent from a controller. During their applications, they might experience cavitation, which is an undesired phenomenon. Cavitation occurs when the local static pressure falls below the vapor pressure in a liquid flow. Valves subjected to cavitation experience noise, erosion, vibrations, choked flow, and damage to the structural integrity of their components [1-5]. This result in plant shutting down, loss of time and capitals [4]. Valve designers have been searching for ways to reduce and/or eliminate cavitation during plant operations. ANSYS FLUENT will be used to investigate cavitation in Ball and Butterfly valve, to obtain an optimal design for each one.

Fossil fuels have been the primary source of energy consumption in our society since the industrial revolution in the 18^{th} century. The Energy Information Agency (EIA) estimates 80% (97.7 quadrillions Btu) of the US energy consumption has been from fossil fuel sources for more than 100 years; 28% is used in the transportation sector [6]. Fossil fuels release greenhouse gases (GHG) that have contributed to global warming and climate change. Environmental concerns over energy use have prompted interest in turning into clean and renewable transportation fuels [7-12]. Biomass is biodegradable and renewable organic matter have been receiving more attention as an alternative to fossil fuels for transportation fuels (gasoline and diesel). Solvent liquefaction is a route currently explored for the conversion of biomass into biofuels. A techno-economic analysis is essential to evaluate its competitiveness against transportation fuels derived from fossil fuels.

References

[1] M. J. Chern, C. C. Wang, and C. H. Ma, "Performance test and flow visualization of ball valve," *Exp. Therm. Fluid Sci.*, vol. 31, no. 6, pp. 505–512, 2007.

[2] S. Bernad, R. F. Susan-Resiga, S. Muntean, and I. Anton, "Cavitation phenomena in hydraulic valves - Numerical modelling," *Proc. Rom. Acad. Ser. A*, vol. 8, no. 2, 2007.

[3] Flowserve, "Flowserve Cavitation Control," pp. 1–20, 2006.

[4] A. Ferrari, "Fluid dynamics of acoustic and hydrodynamic cavitation in hydraulic power systems," 2017.

[5] G. Brett, M. Riveland, T. C. Jensen, and T. J. Heindel, "Cavitation from a Butterfly Valve: Comparing 3D Simulations to 3D X-Ray Computed Tomography Flow Visualization," *Jt. fluids Eng. Conf.*, pp. 1–9, 2011.

[6] B. Li, "Techno-economic and uncertainty analysis of fast pyrolysis and gasification for biofuel production," 2015.

[7] S. Thangalazhy-Gopakumar, S. Adhikari, H. Ravindran, R. B. Gupta, O. Fasina, M. Tu, and S. D. Fernando, "Physiochemical properties of bio-oil produced at various temperatures from pine wood using an auger reactor," *Bioresource. Technol.*, vol. 101, no. 21, pp. 8389–8395, 2010.

[8] R. D. Perlack, B. J. Stokes, L. M. Eaton, and A. F. Turnhollow, "US Billion-ton update. Biomass Supply for a Bioenergy and Bioproducts Industry," *Renewable. Energy*, vol. 7, no. August, pp. 1–229, 2005.

[9] G. Yildiz, F. Ronsse, R. Venderbosch, R. van Duren, S. R. A. Kersten, and W. Prins, "Effect of biomass ash in catalytic fast pyrolysis of pine wood," *Appl. Catalysis. B Environmental*, vol. 168–169, pp. 203–211, 2015.

[10] A. Ferraz, J. Baeza, J. Rodriguez, and J. Freer, "Estimating the chemical composition of biodegraded pine and eucalyptus wood by DRIFT spectroscopy and multivariate analysis," *Bioresource. Technol.*, vol. 74, no. 3, pp. 201–212, 2000.

[11] D. Mohan, C. U. Pittman, M. Bricka, F. Smith, B. Yancey, J. Mohammad, P. H. Steele, M. F. Alexandre-Franco, V. Gómez-Serrano, and H. Gong, "Sorption of arsenic, cadmium, and lead by chars produced from fast pyrolysis of wood and bark during bio-oil production," *J. Colloid Interface Sci.*, vol. 310, no. 1, pp. 57–73, 2007.

[12] Q. Sun, S. Yu, F. Wang, and J. Wang, "Decomposition and gasification of pyrolysis volatiles from pine wood through a bed of hot char," *Fuel*, vol. 90, no. 3, pp. 1041–1048, 2011.

CHAPTER 2. CAVITATION INVESTIGATION IN BALL AND BUTTERFLY VALVE USING COMPUTIONAL FLUID DYNAMICS TECHNIQUE FOR AN OPTIMAL DESIGN

Nzombo D., Wright M., manuscript in preparation

Abstract

Cavitation phenomena are encountered in several engineering applications and devices. It occurs when the local static pressure drops below the liquid vapor pressure within an originally liquid flow; it is generally an undesired phenomenon. Control valves which might experience cavitation are often subject to effects such as noise, erosion, vibrations, choked flow, and damage to the structural integrity of components. Valve walls and the surrounding area can experience localized damage during the collapse and implosion of vapor cavities. This results in a reduction of valve performance and damage to structural integrity. In the industry, most valves reducing cavitation effects are the results of accumulated engineering experience

This study evaluates the possibility of obtaining an optimal design for both a ball and butterfly valve by using Computational Fluid Dynamics (CFD). In this study, we establish parameter correlations, develop a design of experiments, which provides a response surface, and then conduct an optimization of the design. A Multiple-Objective Genetic Algorithm (MOGA) is used for optimization. The optimal ball valve design met a vapor volume fraction of $8.87*10^{-5}$ and a mass flow rate of 0.287 kg/s parameter criteria and a flow domain length of 150 mm; and the optimal butterfly design met a vapor volume fraction of $2.01*10^{-5}$, mass flow rate of 0.291 kg/s, and a flow domain length of 146.9 mm parameter criteria. These designs minimized the potential for cavitation. However, the optimal designs did not meet all constraints suggesting that further work needs to be done to improve these designs.

1. Introduction

Butterfly and ball valves are device that control the flow by varying the size of the flow passage manually or when receiving a signal from a controller. These valves are largely used in the industry, especially to control flow processes of both compressible and incompressible fluids [1-3]. One of the purposes of using them in piping systems is to control flow. Control valves are often used in liquid service and might experience cavitation. Cavitation is described as the formation of vapor bubbles when the local static pressure falls below the saturated vapor pressure.

Valve design consists of a "vena contracta'' (point of narrowest flow restriction) section where the static pressure even at moderate operating conditions can reach a level sufficient for cavitation inception in liquids; at this point, the flow area is smaller compared to the rest of the flow path [3-6]. As the area becomes smaller, at the vena contracta, a transfer of pressure energy causes an increase in velocity, resulting in lower pressures at that region; for most control valves, at the vena contracta, the pressure will fall below the vapor pressure [3-7].

When the local pressure falls below the liquid vapor pressure, bubble formation will start to occur. The pressure recovery in control valves causes bubbles that are filled with vapor and gas to implode once they reach the higher pressure region downstream [3, 5-7]. Valve walls and surrounding area can experience localized damage during the collapse and implosion of vapor cavities. This is an undesired phenomenon and causes a reduction in valve performance and damage to structural integrity.

In the industry, valve designs for reducing cavitation effects are based on accumulated engineering experience; however, cavitation still remains a problem in many

engineering applications and industries [4, 7, 8]. Computational Fluid Dynamics (CFD) is being widely used in the industry and by valve designers to simulate cavitation in control valves, yet there are a limited number of public studies available with experimental data to validate CFD simulations. Cavitation intensity in control valves is commonly evaluated in terms of effects such as noise, erosion, vibrations, choked flow, and damage to the structural integrity of the components. [3, 4, 6-9].

A better understanding of cavitation in both ball and butterfly valve could be improved by employing particle tracking visualization method, and using a specially customized plexiglass tubing to capture and show recirculation regions [4, 8]. Additional techniques of visualizing cavitation include using pressure sensitive films and high-speed photography [4], which gives the possibility of determining the vortex cavitation location responsible for erosion [4, 11, 12]. Bernard and R. Susan-Resiga [11] performed a 3D computational fluid dynamics (CFD) study of cavitational flow inside of a hydraulic poppet valve using the commercial software Fluent V12.0.

Cavitation prediction using simulation techniques still remains a challenge. A method of predicting cavitation in a flow past a cylinder with a square cross-section area using Large-Eddy Simulation (LES) and stability criteria for the cavitation nuclei was developed by Wienken et al. [12]. They obtained significant agreement between the cavitation prediction of their simulations and experimental results.

This study evaluates the possibility of finding an optimal valve design while reducing the adverse effects of cavitation within a flow during valve operation. ANSYS FLUENT V17.1 will be used to select parameters of interest for the current design. The selected parameters are as follow: two different valve geometries (ball and butterfly valve), the pipe

length, fluid properties (pressure inlet and pressure drop), and compared with a range of output parameters (mass flow rate, vapor volume fraction, volumetric flow, and velocity). The aim of this study will consist of determining which design parameters have the most influence and alter them to improve it.

2. Modeling

2.1 Bubble growth and implosion

2.1.1 Bubble formation and dynamics

Cavitation is described as the formation of vapor bubbles when the local static pressure falls below the saturated vapor pressure. Consider a spherical bubble of radius, R (t) (t is time) in where both the temperature and pressure (T_∞ and P_∞) are far away from the bubble. The temperature is assumed to be constant and any uniform heating of the liquid by internal source or radiation are neglected. P_L is the liquid density (constant), r being the radial distance in the liquid from the center of the bubble, S the surface tension, ν_L the liquid kinematic viscosity, U (r, t) the radial outward velocity, and T(r, t) the temperature within the liquid. Pressure (known or controlled) is the physical force regulating the growth and/or collapse of the bubble [9]. Additional assumptions are made: the density of the liquid is constant and the dynamic viscosity is constant and uniform. The contents of the bubble are homogenous, while the temperature and pressure within the bubble are uniform. In the presence of mass transport across boundaries (evaporation and condensation), the bubble dynamics is described by the generalized form of the Rayleigh-Plesset equation (1). Figure 1 shows the image of a spherical bubble in an infinite liquid.

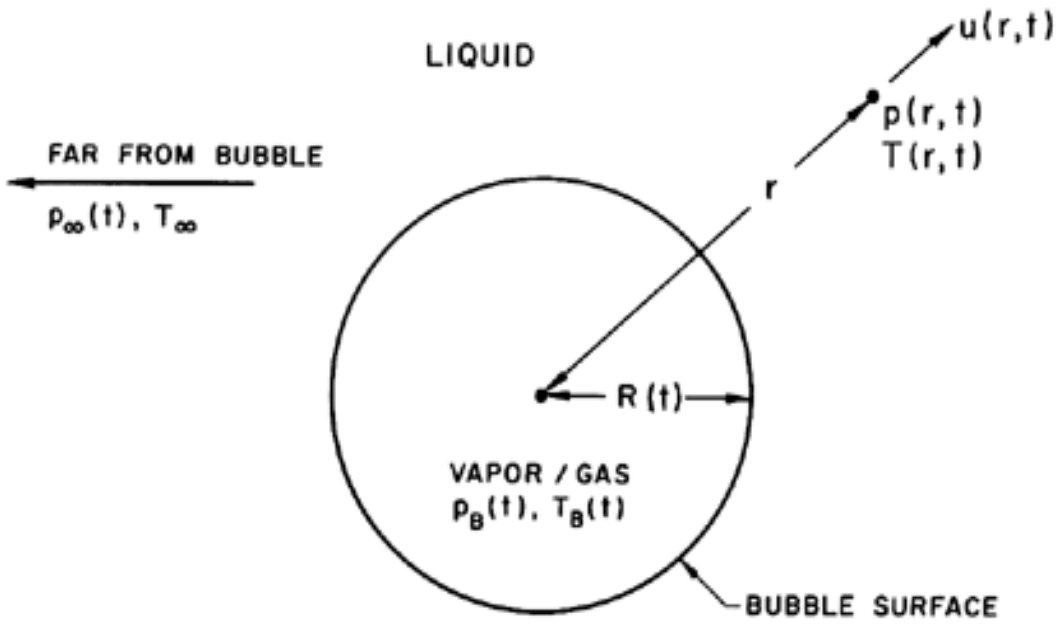

Figure 1: Schematic of a spherical bubble in an infinite liquid, copied from [9].

$$\frac{P_B(t)-P_\infty(t)}{\rho_L} = R\frac{d^2R}{dt^2} + \frac{3}{2}\left(\frac{dR}{dt}\right)^2 + \frac{4\nu_L}{R}\frac{dR}{dR} + \frac{2S}{\rho_L R} \quad (1)$$

2.1.2 Bubble implosion

The formation of bubbles occurs when the local pressure drops below the vapor pressure within a flow. When the pressure recovers, bubbles filled with vapor and gases have high kinetic energy and velocities, and will implode when reaching higher pressure zones [2, 10-11]. Pressure gradient in ambient fluid or the influence of rigid boundaries causes cavitation bubbles to change from its spherical symmetric shape before imploding and forming micro jets [3, 5, 9]. Figure 2 and 3, respectively, shows the image of a bubble growth in a superheated droplet, and vapor-filled cavitation bubble in the trailing edge of a foil. Figure 4 shows the image of bubble moving into a higher pressure region and collapsing near the wall of a rigid boundary.

Figure 2: Bubble formation and growth, copied from [9].

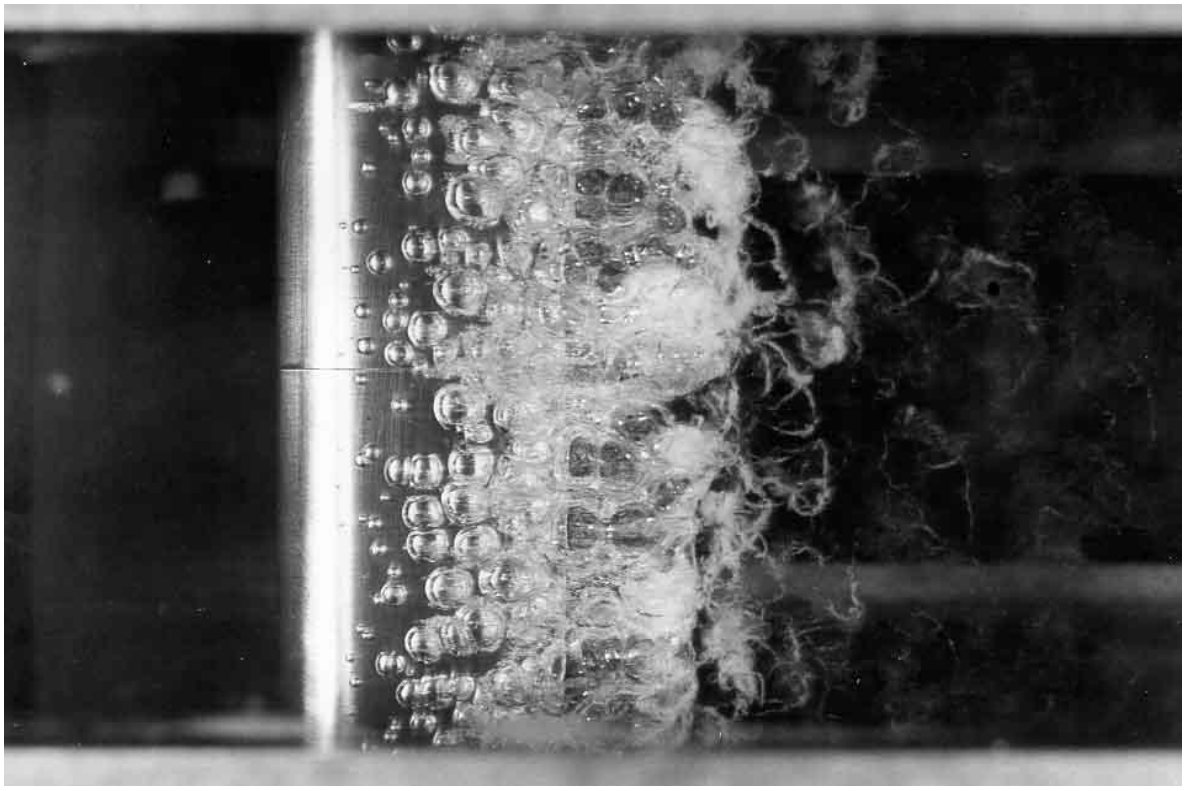

Figure 3: Dense traveling cavitation on the surface, copied from [9].

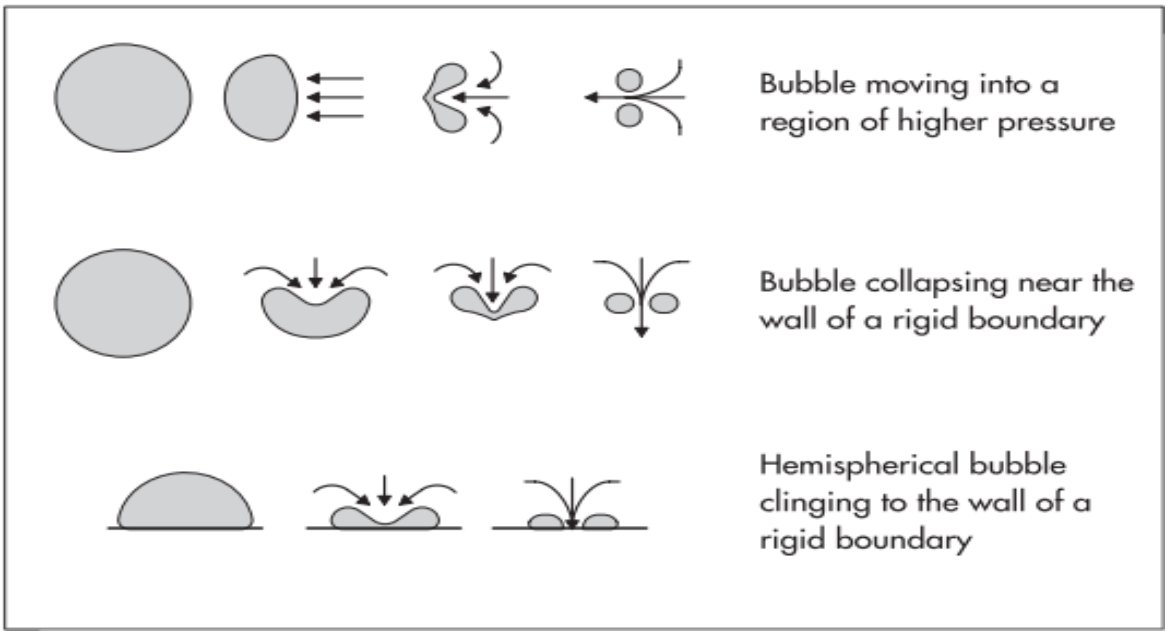

Figure 4: Bubble collapsing and microjet formation, copied from [3].

2.2 Physical modeling

The present cavitation model is based on the following physical assumptions: cavitation is modeled as the growth and collapse process of vapor bubbles. The system investigated consists of a liquid and vapor phase coupled as a mixture. The mixture model used in this study for the numerical simulation of cavitating flows is from ANSYS FLUENT V17.1 code [13, 14]. Due to its large use for engineering applications in both industrial and academic settings, ANSYS-FLUENT is the commercial CFD code chosen to investigate cavitation in this study. This is a simplified multiphase model used to model homogeneous flows with great coupling capabilities where each phase (liquid and vapor) moves at the same velocity [8, 13, 14]. The flow is assumed to be in thermal and dynamic equilibrium and the

velocity continuous. Lastly, the mixture is modeled as an incompressible flow and all density changes are neglected.

2.3 Governing equations

In the present study, the mixture is composed of the liquid water and vapor predicted using the cavitation model. It is modeled as homogeneous flows where each phase is assumed to move at the same velocity. The mixture model of both phases solve the main CFD equations of continuity, momentum, and energy [7, 16-18].

The continuity equation for the mixture is described as:

$$\frac{\partial}{\partial t}(\rho_m) + \nabla.(\rho_m \vec{V}_m) = 0 \quad (2)$$

$\overrightarrow{V_m}$ is the local mass-averaged velocity is:

$$\overrightarrow{V_m} = \frac{\sum_{k=1}^{2} \alpha_k \rho_k \overrightarrow{V_k}}{\rho_m} \quad (3)$$

ρ_m is the mixture density described as:

$$\rho_m = \sum_{k=1}^{2} \alpha_k \rho_k \quad (4)$$

α_k is defined as the volume fraction of phase k. The two phases involved are liquid water and water vapor. The momentum equation for the mixture is the sum of the momentum equation of each phase (liquid and vapor), and it is described as:

$$\frac{\partial}{\partial t}\left(\rho_m \vec{V}_m\right) + \nabla.\left(\rho_m \vec{V}_m \vec{V}_m\right) = -\nabla \mathrm{p} + \nabla.\left[\mu_m\left(\nabla \vec{V}_m + \vec{V}_m\right)\right] + \rho_m \vec{g} + \vec{F} +$$

$$\nabla.\left(\sum_{k=1}^{2} \alpha_k \rho_k \vec{V}_{dr,k} \vec{V}_{dr,k}\right) \quad (5)$$

$\vec{F}$ and μ_m are respectively the body force and the mixture viscosity.

$$\mu_m = \sum_{k=1}^{2} \alpha_k \mu_k \quad (6)$$

$\vec{V}_{dr,k}$ is the drift velocity for the vapor phase (7)

The energy equation for the mixture is described as:

$$\frac{\partial}{\partial t}\sum_{k=1}^{2}(\alpha_k \rho_k E_k) + \nabla.\sum_{k=1}^{2}(\alpha_k v_k(\rho_k E_k + p)) = \nabla.\left(K_{eff}\nabla \mathrm{T}\right) + S_E \quad (8)$$

Where K_{eff} is the effective conductivity

$E_k = h_k$ (Incompressible phase) (10)

h_k is the sensible enthalpy for phase k

2.4 Numerical Method

The cavitation simulation in this study was conducted by using the numerical code in FLUENT V17.1 [14]. The code uses the finite control volume (FCV) method, which requires solving the problem of interest by spatial discretization of the domain from generated meshes [15, 16]. This technique converts the governing equations into algebraic equations to be solved numerically. The governing equations are integrated for each control volume, resulting in discrete equations converting each quantity on a control-volume basis. In this approach, surface and volume integrals are approximated and values from cell centers are interpolated to cell faces [15, 16]. The governing equations for mass, momentum, and energy are solved sequentially [16].

With transient problems, the approach of obtaining the solution is by marching time; the time domain is broken into a finite number of time steps. In ANSYS FLUENT, discretization of the solution domain creates a computational mesh with finite number of control volumes, and discretized governing equations are solved [15, 16].

2.5 Cavitation Flow Modeling

Cavitating flows are sensitive to vapor bubble formation and transport, turbulent fluctuations of pressure and velocity, and the magnitude of non-condensable gases that are dissolved in the liquid [12, 14-20]. The numerical simulation of two-phase cavitating flows is

a research area still in exploration, for which the aspiring goal is to compute the unsteady evolution for the growth and collapse of cavities [18-24]. A set of practical computations used in industrial flows with Reynolds-averaged Navier-Stokes (RANS) code has been developed by the CFD community [21, 22, 25-29]. This code is used in different commercial code and software such as AUTODESK, COMSOL, FLUENT, etc. All numerical simulation in this study was conducted using FLUENT V17.1.

The cavitation model in FLUENT V17.1 has the following capabilities: the cavitation models can be applied to any geometry, all grid types supported in FLUENT V17.1, non-conformal sliding interfaces, and moving and/or deforming mesh. The models can be solved with mixture (mixture model) or phase (Eulerian multifluid) temperature equations [14, 28]. FLUENT V17.1 extends the models to multiphase and multi-species systems. All turbulence models are totally compatible in FLUENT, ranging from simple length scale models to large eddy simulation (LES) [7, 14, 28]. Both liquid and vapor phase can be incompressible or compressible. The input material properties (vaporization pressure, density, viscosity, and etc.) can be constants or functions of temperature. The mass transfer between the liquid and vapor phase is assumed to take place. Both bubble formation (evaporation) and collapse (condensation) are taken into account in the cavitation models. The positive mass transfer is from the liquid to the vapor. Lastly, the cavitation models are based on the Rayleigh-Plesset equation, describing the growth of a single vapor bubble in a liquid [14].

2.6 Vapor Generation Modeling

The Schnerr and Sauer [15] model is used to predict cavitation. The net mass transfer from liquid to vapor is governed by the equation for the vapor volume fraction:

$$\frac{\partial}{\partial t}(\alpha\rho_v) + \nabla.\left(\alpha\rho_v\vec{V_v}\right) = \frac{\rho_v\rho_l}{\rho}\frac{D\alpha}{Dt} \qquad (8)$$

The net mass transfer is described as:

$$R = \frac{\rho_V \rho_l D_\alpha}{\rho\, Dt} \tag{9}$$

Schnerr and Sauer [12] connects the vapor volume fraction to the number of bubbles, n_b, per volume of liquid by the following expression:

$$\alpha = \frac{n_b \frac{4}{3}\pi(\Re^3{}_B)}{1+n_b \frac{4}{3}\pi(\Re^3{}_B)} \tag{10}$$

$\Re_B$ is the bubble radius. The final form of the mass source is described by the following equations:

When $P_v \geq P$

$$R_e = \frac{\rho_v \rho_l}{\rho}\alpha(1-\alpha)\frac{3}{\Re_B}\sqrt{\frac{2\,(P_v - P)}{3\,\rho_l}} \tag{11}$$

and when $P_v \leq P$

$$R_c = \frac{\rho_v \rho_l}{\rho}\alpha(1-\alpha)\frac{3}{\Re_B}\sqrt{\frac{2\,(P_v - P)}{3\,\rho_l}} \tag{12}$$

P_v is the vapor pressure and P is the local static pressure. The bubble radius is described as:

$$\Re_B = \left(\frac{\alpha}{1-\alpha}\,\frac{3}{4\pi}\,\frac{1}{n_b}\right)^{\frac{1}{3}} \tag{13}$$

The FLUENT V17.1 model requires that the materials present in the simulation be defined as a liquid and vapor [7, 14]. The vapor was defined as the mixture of 2 species: water and vapor. The fluid phase properties are defined in Table 1.

Table 1: Fluid phase properties (liquid and vapor).

Fluid phase	Density (Kg/m^3)	Viscosity (Kg/m-s)	Mass diffusivity (m^2/s)	Specific heat (J/Kg-K)
Water-liquid	1000	$1.0*10^{-3}$	----------	1006
Water-vapor	0.554	$1.34*10^{-5}$	$2.88*10^{-5}$	----------

3. Methodology

3.1 Ball and Butterfly Valve Modeling

Ball and butterfly valves are devices that control the flow by varying the size of the flow passage manually or when receiving a signal from a controller. Unlike sliding stem valves, they do not have many components such as stem, bonnet, cage, etc. A ball valve typically has a metal disc, but unlike the butterfly valve, it does not have a shaft around which it can rotate. Figure 5 represents a ball valve, and Figure 6 represents its simplified geometry as used in this study. Figure 7 shows a butterfly valve, and the simplified geometry version shown on Figure 8 will be used for simulation. For the sake of saving computational time and resources, the simplified geometry of both the ball valve and butterfly valve were modeled in ANSYS design modeler as shown in Figure 6 and 7. Both valves have a disc which has an opening angle ranging from 0° to 90°. These valves are largely used in the industry, especially for controlling flow processes of both compressible and incompressible fluids [6, 7, 11, 30].

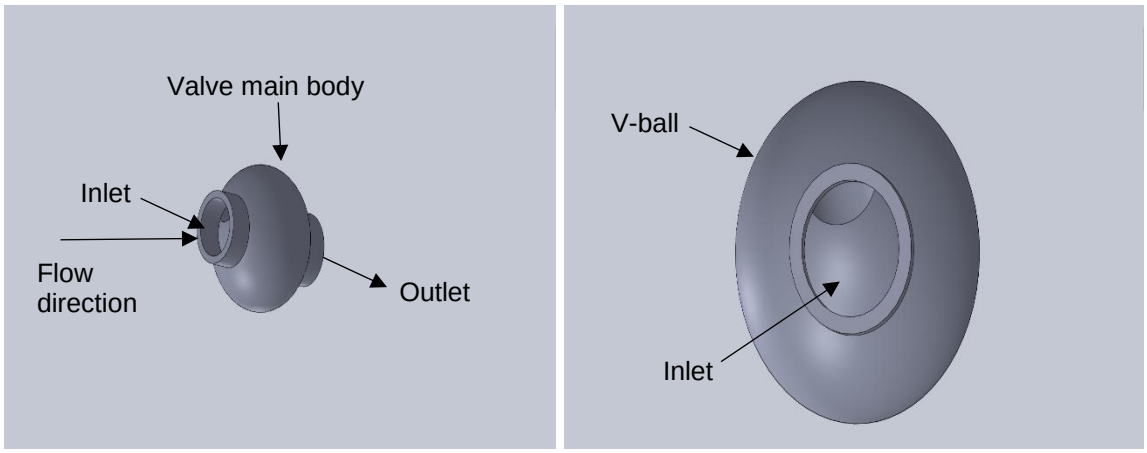

Figure 5: Ball valve (left) and close of up view (right) of its interior.

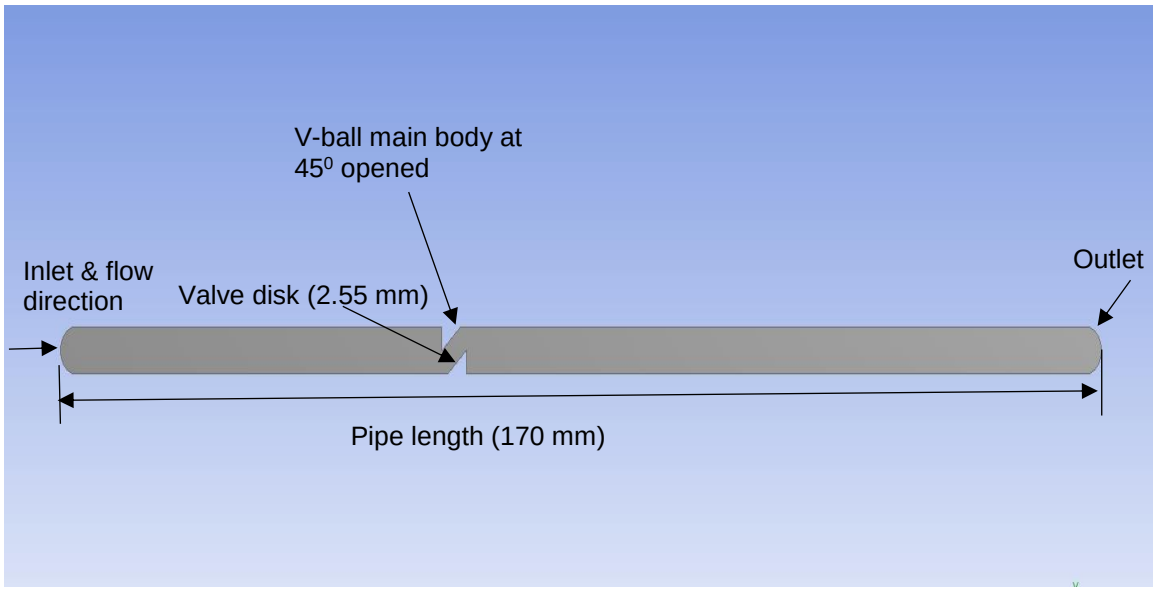

Figure 6: Simplified geometry of ball valve used to simulate cavitation.

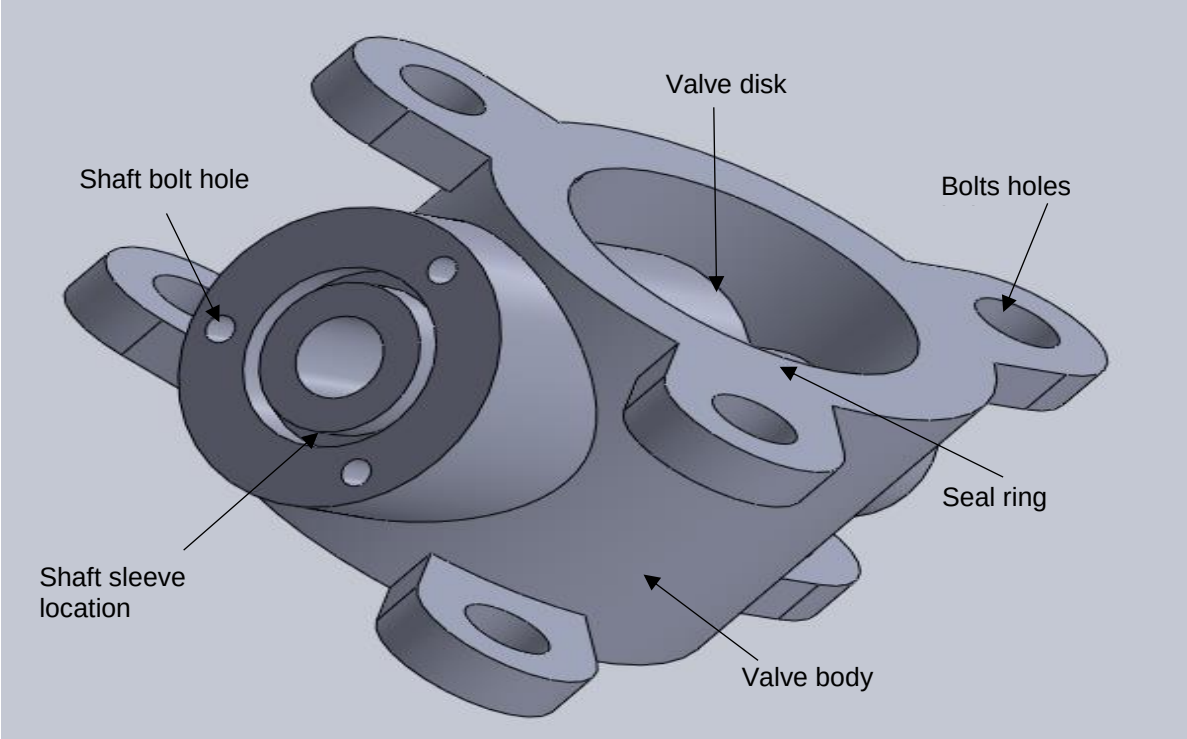

Figure 7: Butterfly valve geometry.

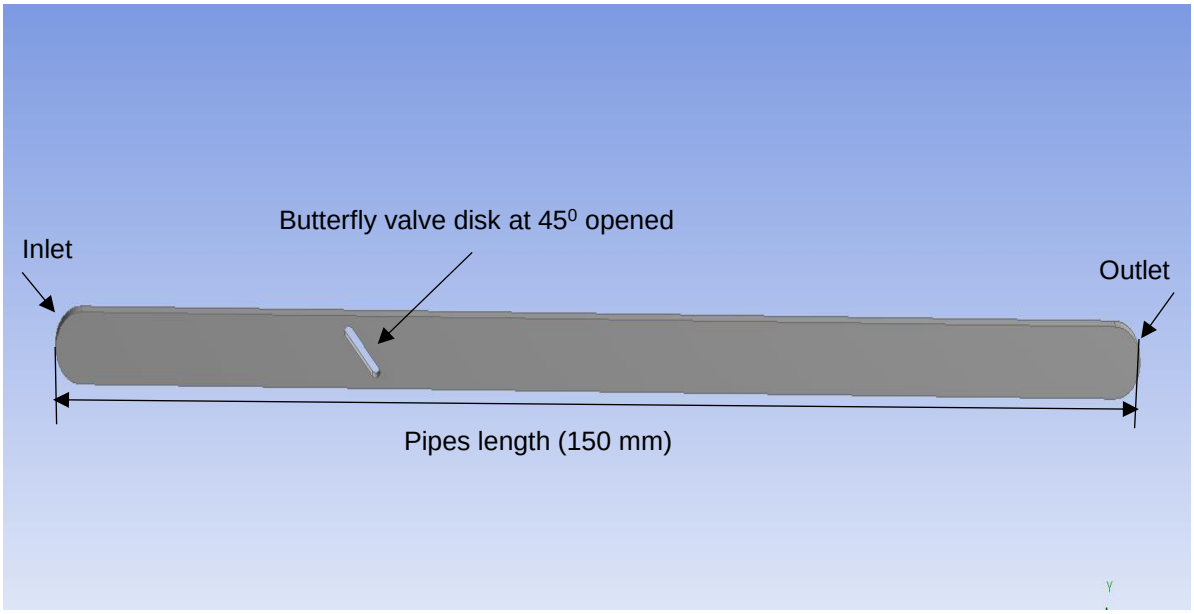

Figure 8: Simplified geometry of butterfly valve used to simulate cavitation.

3.2 Grid Resolution and Simulation

3.2.1 Valve meshing technique

In order to numerically solve the phenomena being investigated in this study, it is necessary to discretize the continuous medium into discrete volumetric cells, consisting of vertices and cells. All areas considered in the flow domain must be captured to accurately model the valve geometry; these include the valve, upstream and downstream piping sections, and the flow physics [7, 15, 31-33]. The computational mesh process in ANSYS consists of selecting correct meshing models, changing the mesh sizing parameters locally and/or globally, setting volumetric controls, and running the surface and/or volume mesh controls. Failure of going through these steps will result in not getting convergence and/or inaccuracy of the simulation results [7, 15, 23]. Due to the limited computing resources and time available, a simplified geometry of each valve was modeled.

3.2.2 Butterfly valve meshing

The dimensions of the geometry were as follow: the inlet and outlet diameter was 7 mm, the inlet to the valve disk was 42 mm (6D) and the outlet to the valve was 105 mm (15D), the distance between the valve disk with the top and bottom wall was 3mm (1.5 m on each side) the disk thickness was 3 mm, the vertical distance between the top and bottom wall was 7 mm, extruded at 5 mm, and the entire length of the computational domain (pipes length and valve) was 150 mm (21.5 D). The butterfly valve geometry offers the opportunity of taking advantage of its symmetry to reduce the simulation complexity and therefore, one-half of the valve was modeled with the disk opened at 45°. The entire flow physics was capture in the meshing process.

The meshing method used was sweeping, which consists of hexahedral elements used for the valve and piping sections of the model shown in Figure 8 and 9. Additional meshing

specifications included: element size of 0.25 mm (0.16% of the flow domain length), the total thickness option with 12 layers and a transition ratio of 0.272 was selected to capture the effect of the boundary layer on the walls, and a growth rate of 1.2. A high-quality mesh is required to simulate a multiphase cavitation flow and obtain a converged result. The program generated 220,259 computational cells and 246,232 nodes; the mesh quality used in this study had a maximum element skewness of 0.72 (less than 1 is good quality), a maximum orthogonal quality was 1 (best quality), and a maximum element of 1 [15].

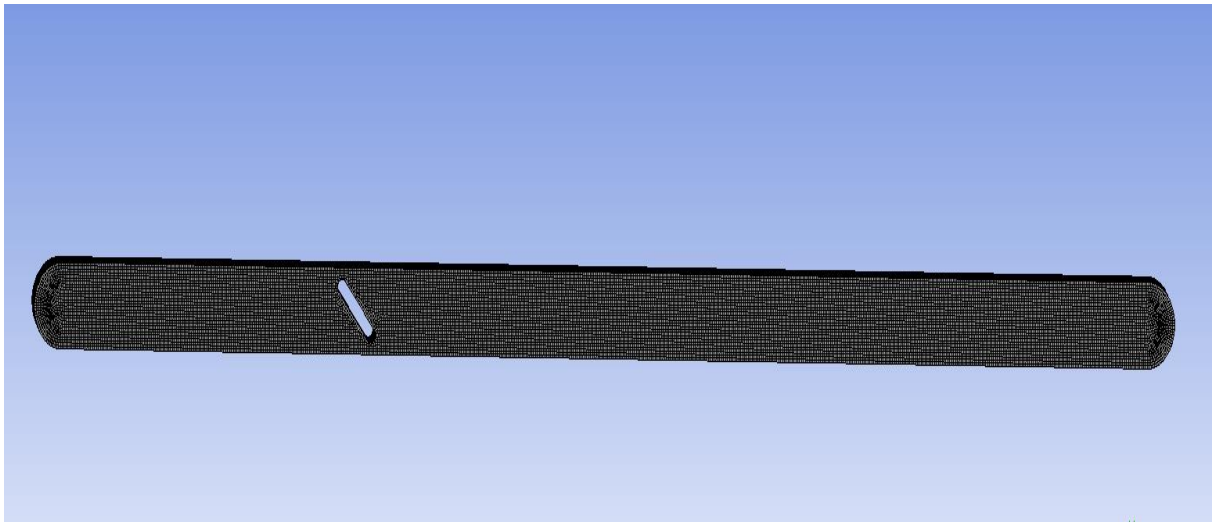

Figure 9: Simplified geometry of butterfly valve with hexahedral mesh and disk open at 45˚.

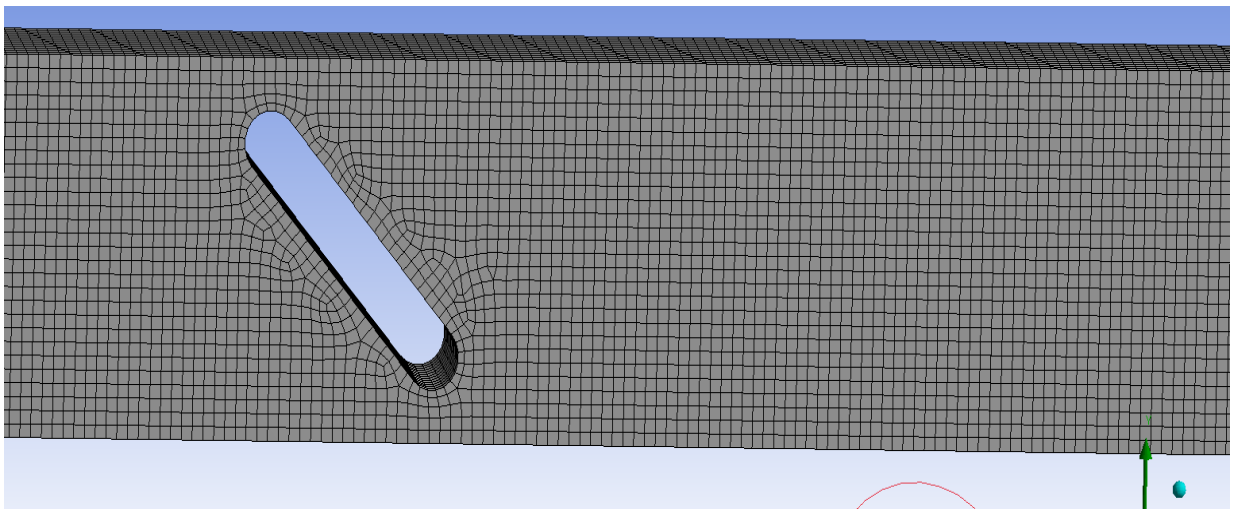

Figure 10: Hexahedral mesh close-up of butterfly valve with a disk open at 45˚.

3.2.3 Ball valve meshing

The dimensions of the ball valve geometry were as follow: the inlet and outlet diameter was 5 mm, the inlet to the valve was 61 mm (12D) and the outlet to the valve was 106 mm (21D), the valve thickness was 3 mm, the vertical distance between the top and bottom wall was 5 mm, extruded at 5 mm, and the entire length the computational domain was 170 mm (34D). The ball valve geometry is symmetrical and thus, one-half of the valve was modeled with a disk opened at 45°. The entire flow physics was capture in the meshing process.

The meshing method used was sweeping, which consists of hexahedral elements used for the valve and piping sections of the model shown in Figure 11 and 12. Additional meshing specifications included: element size of 0.25 mm (0.14% of the flow domain length), the total thickness option with 12 layers and a transition ratio of 0.272 was selected to capture the effect of the boundary layer on the walls, and a growth rate of 1.2. A high-quality mesh is required to simulate a multiphase cavitation flow and obtain a converged result. The program generated 107,720 computational cells and 127,413 nodes; the mesh quality used in this study had a maximum element skewness of 0.54 (great quality), a maximum orthogonal quality was 1 (best quality), and a maximum element of 1 [15].

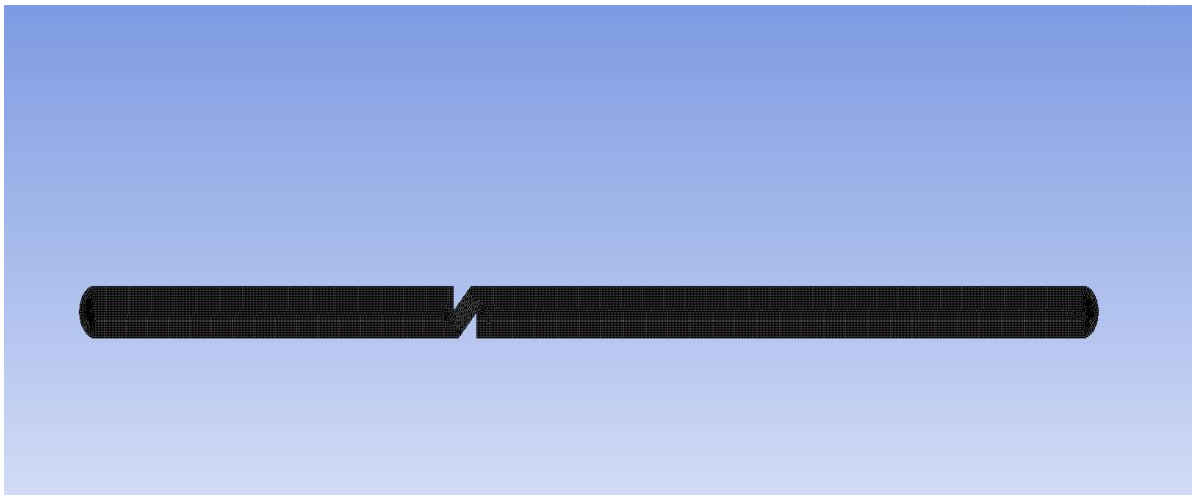

Figure 11: Simplified geometry of ball valve with hexahedral mesh and disk open at 45°.

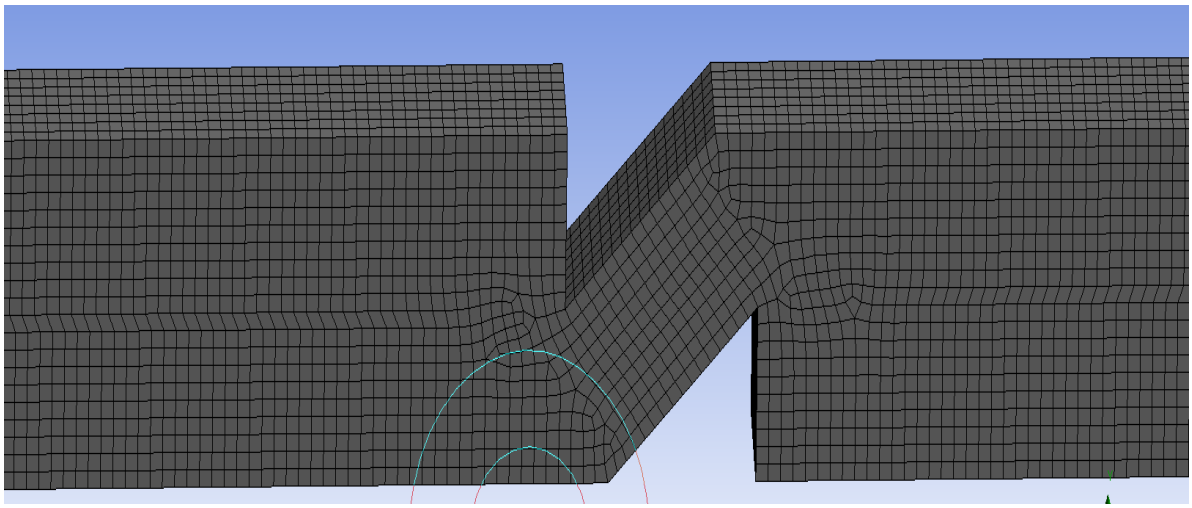

Figure 12: Hexahedral mesh closed up of ball valve with a disk 45°.

3.3 Boundary conditions

The assumptions and conditions used in this study were similar for both types of valves. The fluid was at a fixed temperature of 300 K and the velocity profile was assumed uniform throughout the flow. The inlet pressure was varied at different values, while the outlet pressure remained at a fixed value. The no-slip condition was applied for the velocity at the wall (top and bottom) and other solid surfaces. The software requires material used in the simulation to be clearly defined in FLUENT V17.1. The phases are defined as liquid and

vapor, and Table 2 shows the boundary conditions, fluid properties, and cavitation models used in this study. Table 3 shows the scheme selection and monitors values used in this simulation.

Table 2: Boundary conditions, fluid properties, and cavitation model

Boundary type	Interface
Multiphase model	Mixture with 2 eulerian phases
Viscous	Realizable K-e, standard wall functions
Velocity	Uniform
Pressure inlet	3, 6 bar
Pressure outlet	1 bar
Water-liquid	@ 300 K
Water-vapor	@ 298 K
Specification method (inlet & outlet)	k-ε
Turbulent Kinetic energy (inlet & outlet)	0.02 m^2/s^2
Relaxation factor	0.95
Turbulent dissipation rate (inlet & outlet)	1 m^2/s^3
Water-liquid density	1000 kg/m^3
Water-liquid viscosity	0.001 kg/ms
Water-vapor density	0.02558 kg/m^3
Water-vapor viscosity	$1.26*10^{-^6}$ kg/ms
Wall conditions	No slip
Thermal conductivity	0.0261 W/mK
Cavitation model	Schnerr-Sauer

Table 3: Scheme selection and residual monitors' values

Scheme	Coupled
Pressure	Presto
Momentum	Quick
Volume fraction	Quick
Turbulent kinetic energy	First Order Upwind
Turbulent dissipation rate	First Order Upwind
Continuity	3e-07
X-Velocity	1e-05
Y-Velocity	1e-05
Z-Velocity	1e-05
k	1e-05
ε	1e-05
Vf-vapor	0.001

3.4 Numerical Procedure for Solution

For a rigorous computation, the transient calculation is required for the simulation of the irregular cyclic process of bubble formation, growth and collapse, and water jet-re-entry. Initial attempts of performing steady state calculations were unsuccessful. Different adjustments were made with the purpose of getting a converged solution. They included increasing the length of the flow domain from 120 mm to 150 mm, changing the meshing method originally tetrahedral to hexahedral, and varying the relaxation factor from 0.75 to 0.95. The adjustments slightly improved the simulation but did not result in a converged solution. Additional changes in the simulation were made by changing the solver time from steady state to transient solution. A time step size of $2.5*10^{-5}$ seconds was introduced in the simulation and a maximum number of iterations per time step. These adjustments resulted in getting a converged solution of the flow simulation.

4. Results and Discussion

4.1 Cavitation Flow Simulation and Analysis

Two main simulations cases were completed for both valves with the same flow conditions. Under both flow conditions, the pressure outlet was kept fixed at 1 bar, while the inlet pressure values used were 3 and 6 bar. These conditions provided two different pressure drop values, which under the first scenario was 2 bar and 5 bar on the second. The ratio of the pressure drop of more than 1:2 is intended to clearly identify the turbulence effects on the cavitation flow. Additionally, the temperature of the fluid in the flow was 300 K (27° C). Greater turbulence and vapor volume fraction were observed at higher pressure, while the inlet pressure was at 6 bar.

4.2 Butterfly design

The butterfly valve design consisted of different considerations under which the expected outcome is an optimal design. The first consideration was the pressure used for the investigation. Figure 13 is the pressure contour showing location of low and high pressure in the butterfly valve. Since cavitation flow is an unsteady phenomenon, it is important to observe the influence of turbulent effects, then account for it in design optimization [2, 36-40]. Figure 14 is the turbulent kinetic energy contour, showing the location of high turbulence in the flow. Figure 15 and 16, respectively, shows the vapor volume fraction occurring at the disk edge in and the highest velocity is observed in the vena contracta region at the edge of the valve disk.

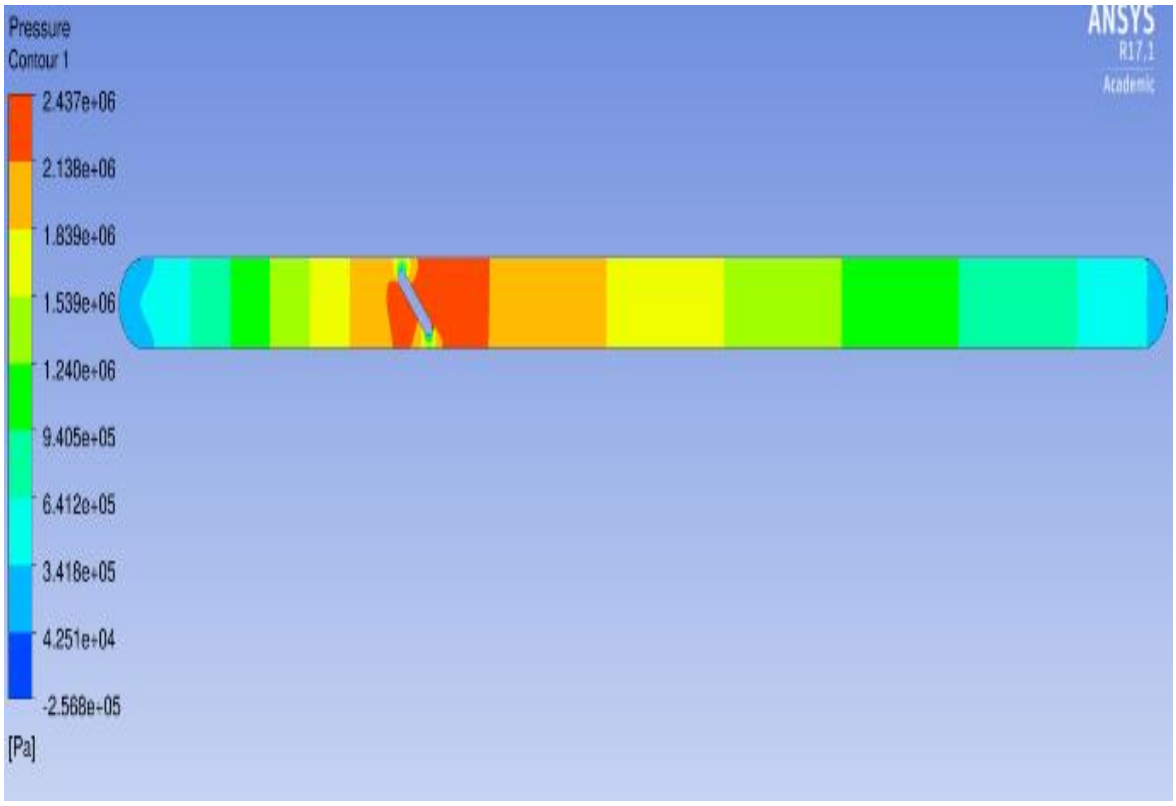

Figure 13: Butterfly valve pressure inlet contour at 3 bar.

The fluid passage in the vena contracta causes the local pressure to fall below the vapor pressure and the velocity to increase. This resulted in stronger turbulence effects and vapor volume fraction (cavitation) at the disk edge.

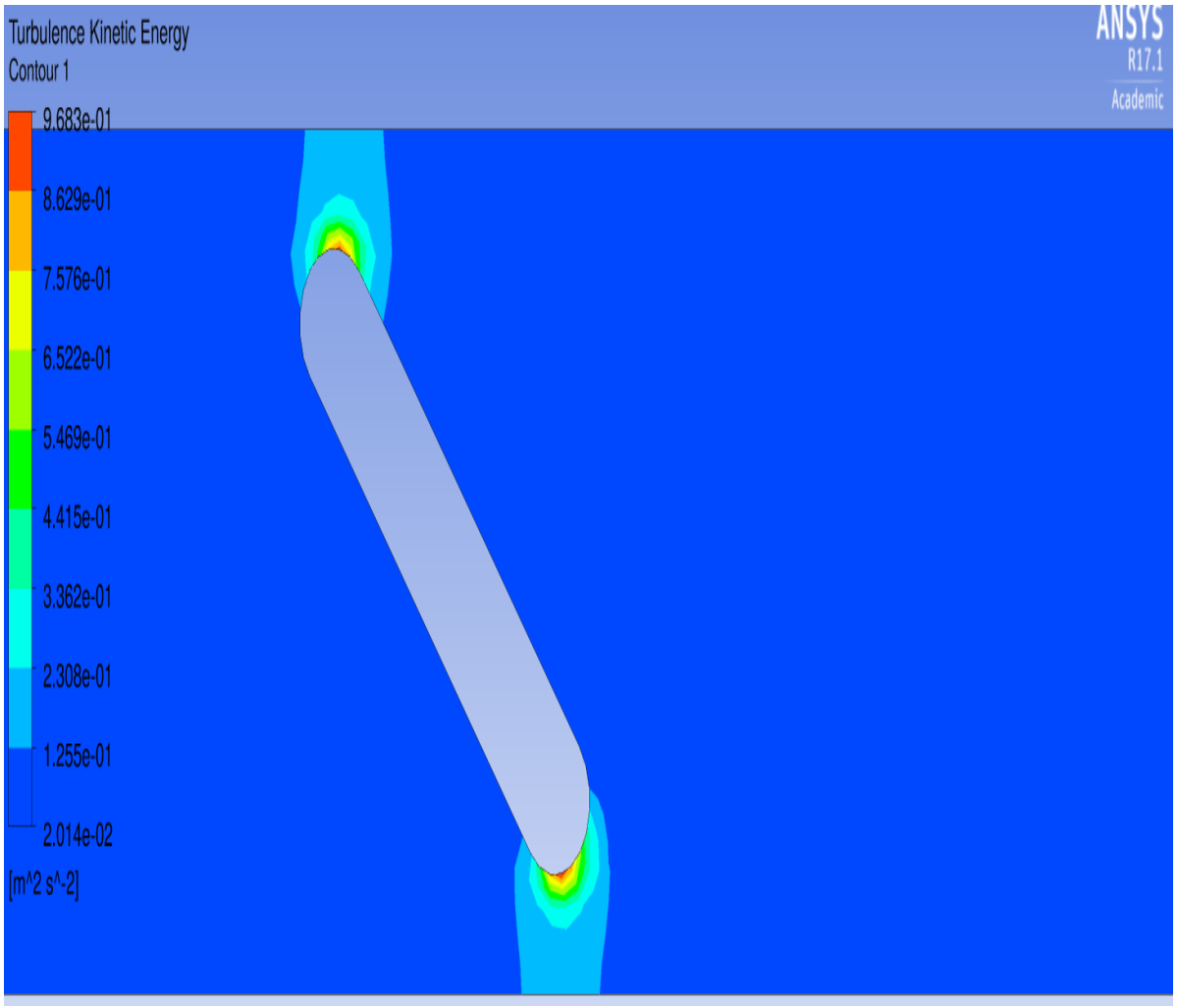

Figure 14: Butterfly valve turbulent kinetic energy contour at 3 bar.

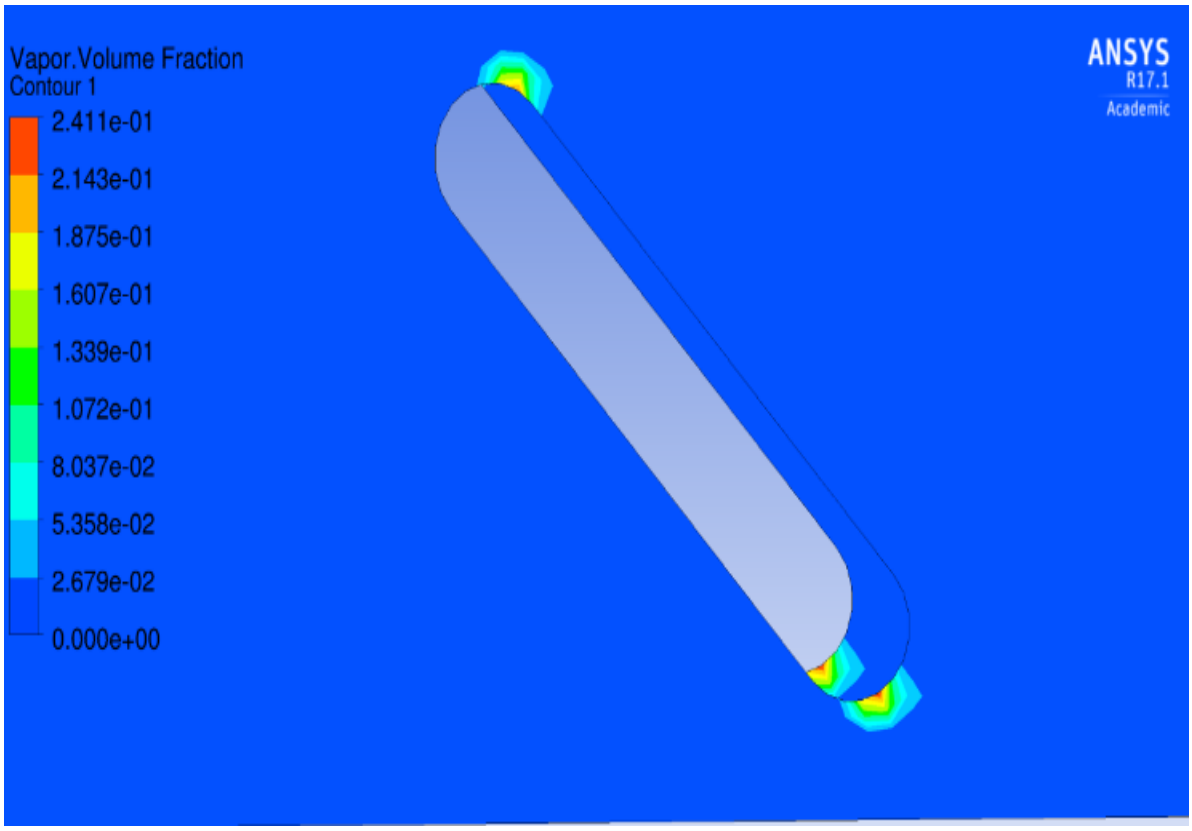

Figure 15: Butterfly valve vapor volume fraction (cavitation) region in the flow at 3 bar.

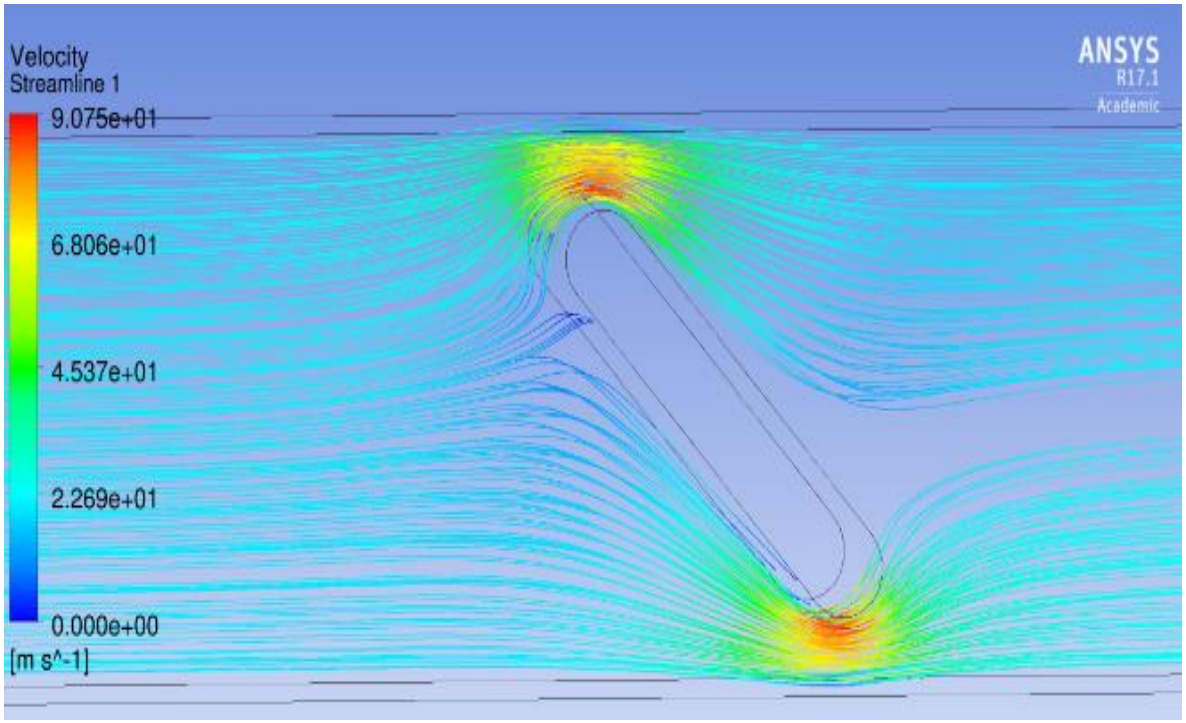

Figure 16: Butterfly valve velocity streamlines contour in the vena contracta.

4.2.1 Butterfly design set up and optimization

In order to achieve a decent butterfly valve design, the above observations and design consideration must be accounted for during the design of the experiment. The first step was to determine which parameters had the greatest influence on the design. ANSYS FLUENT V17.1 provides different options for generating a robust design without having experimental data [29]. It consists of examining all the parameters involved in the design, then setting a design of experiment, getting a response surface, and a response surface optimization. Figure 17 shows a schematic of all the design process and different tabs for each design step used in FLUENT.

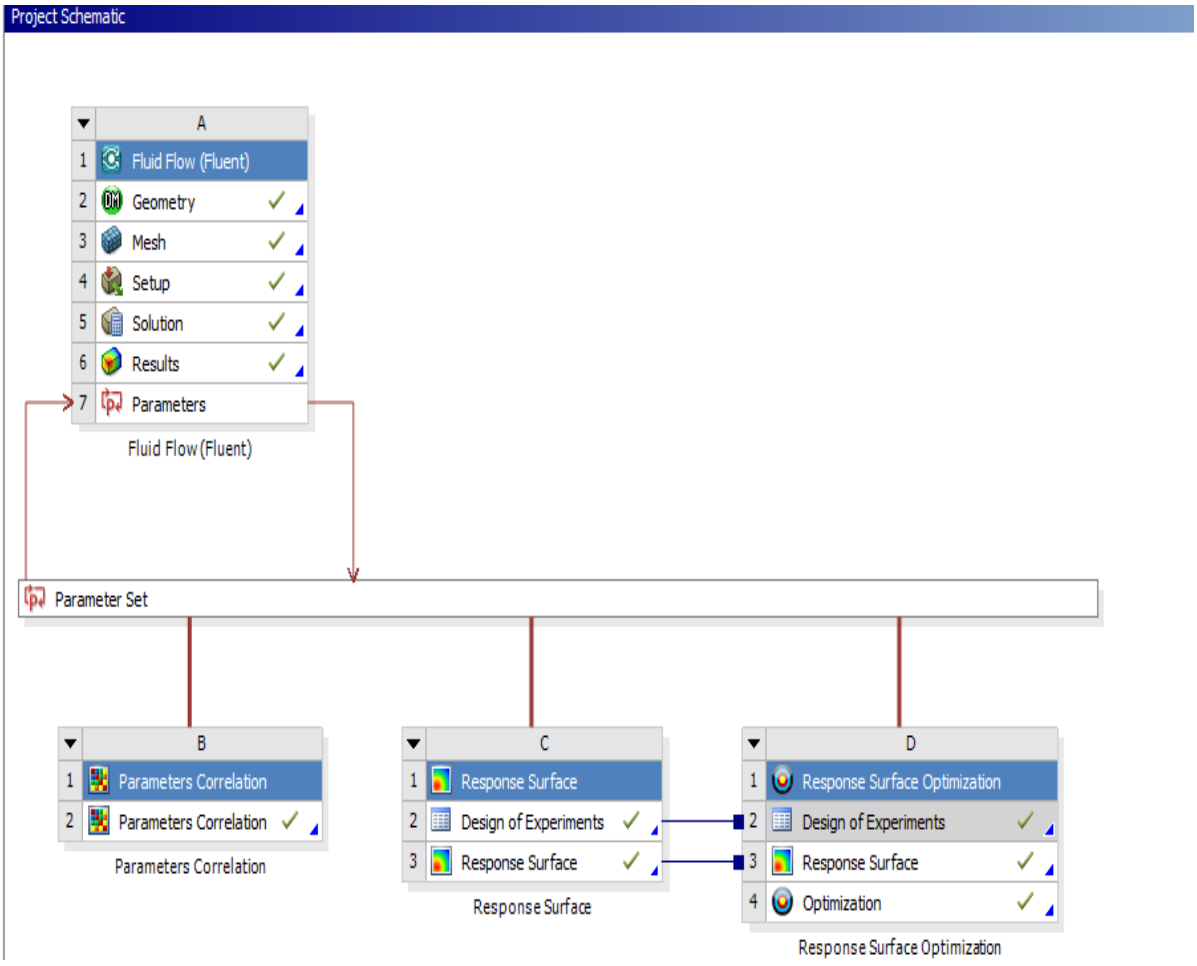

Figure 17: Project schematic to determine parameter correlation, design of experiment (DOE), response surface, and response surface optimization (RSO).

Figure 18 shows which parameters have the most influence on the design, which are determined based on the input and output parameters, and how they affect the design. Based on this information, a design of experiments can be set up within a fixed range, where both the lower and upper value of a parameter is determined. Parameter correlation (Figure 18) generates a heat map assessing how inputs affect outputs. Dark (red) color signifies any change in the input directly affect the output, while blue shows an inverse relationship; parameters in the gray area have no effect and the numerical value associated with them is almost zero. Therefore, the major parameters of interests are position (input) and mass flow rate (output), followed by pressure inlet and pressure drop. The mass flow rate is inversely proportional to the position (valve and pipes length), meaning an increase in position will decrease the mass flow rate.

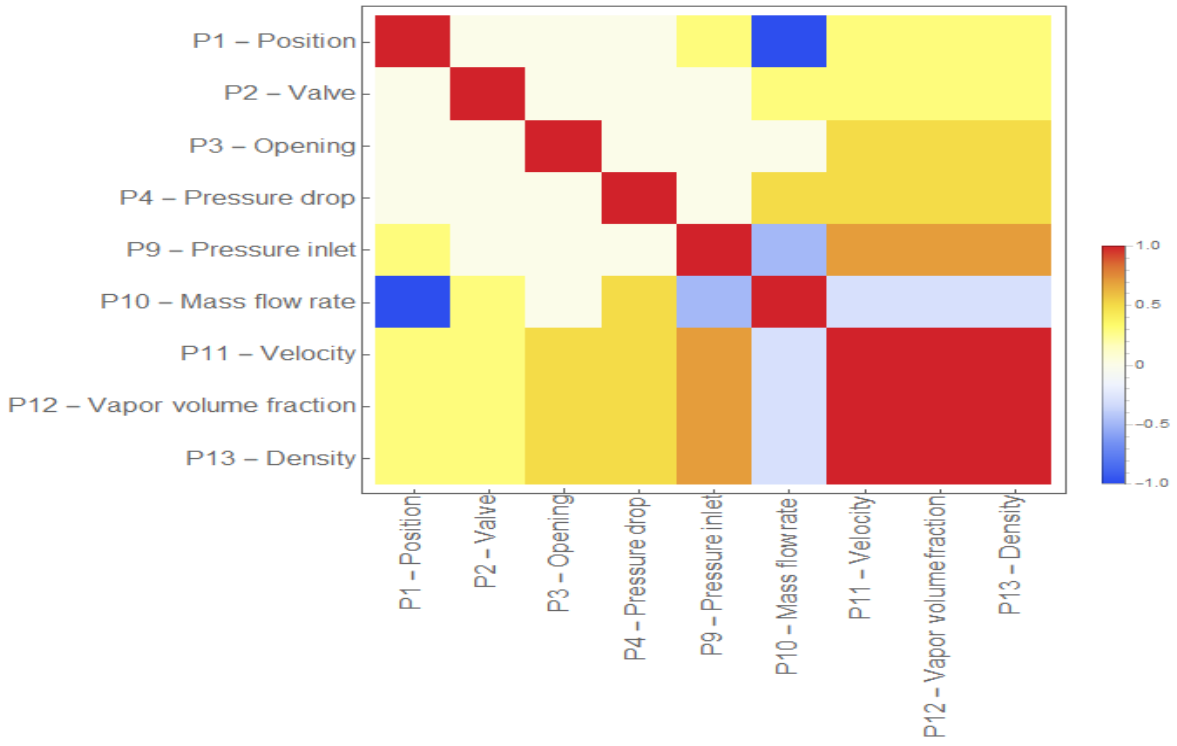

Figure 18: Parameters correlation for Butterfly valve design improvement.

The design of experiment takes inputs from parameter correlation results and distributes sample points bounded within a design space. The lower and upper bounds of input parameters are defined and optimize the sampling of the design space. When the DOE is completed, the response surface is used to predict results at any point within the chosen design. ANSYS uses a system of stars to check the validity of both a response surface and design optimization. 3stars signify that the design meet all the criteria, 2stars meaning about 2/3 of the criteria are met, and 1 star for a poor design. Additionally, a gray bar means it is neutral, and XXX attributed to the worst design.

Table 4 shows the response surface of the design of experiment conducted on the butterfly valve. With the current response surface, the butterfly valve design is poor and therefore needs optimization. In order to improve this design, FLUENT requires selecting at least 3 parameters (input and output), seeking a target, minimizing or maximizing a given parameter for getting different design options. A Multiple-Objective Genetic Algorithm (MOGA) is used to address weaknesses of the current design and improve other parameters. Table 4 and 5, respectively, shows the response surface and the response surface optimization with constraints and target.

Table 4: Response surface of butterfly valve design

	P12 - Mass flow rate	P12 - Vapor volume fraction	P14 - Velocity	P15 - Density	Numerical value (star)
Coefficient of Determination (Best Value = 1)					
Learning Points	1	1	1	1	3
Cross-Validation on Learning Points	0	1	1	1	
Root Mean Square Error (Best Value = 0)					
Learning Points	0	$8.62*10^{-15}$	$5.83*10^{-21}$	$1.63*10^{-3}$	0
Verification Points	0	$1.06*10^{-14}$	$6.77*10^{-21}$	1.3*10-3	0
Cross-Validation on Learning Points	0	10^{-3}	$7.79*10^{6}$	$7*10^{-3}$	0
Relative Maximum Absolute Error (Best Value = 0%)					
Learning Points	0	0	0	0	XXX (P12)
Verification Points	0	0	0	412.3	Neutral
Cross-Validation on Learning Points	417.3	0	0	412.3	XXX (P12)
Relative Average Absolute Error (Best Value = 0%)					
Learning Points	0	12.5	12.5	12.5	Neutral (P12)
Verification Points	0	7.74	7.74	7.74	2 (P12)
Cross-Validation on Learning Points	$4.16*10^{-13}$ (XX)	63.6	63.6	63.6	XX

Table 5: Design parameter optimization from response surface of butterfly design

Optimization study					
Maximize P14	Goal, maximize P14				
Seek P12= $2.01*10^{-5}$	Goal, seek P13				
Minimize P16	Goal, minimize P16				
Optimization method					
MOGA	The MOGA method (Multi-Objective Genetic Algorithm) supports multiple objectives and constraints and aims at finding the global optimum				
Configuration	Generate 1000 samples initially, 100 samples and find 5 candidates in maximum of 20 iterations				
Status	Converged after 1504 evaluations				
Candidate points					
	Candidate point 1	**Candidate point 2**	**Candidate point 3**	**Candidate point 4**	**Candidate point 5**
P1 position (mm)	**145**	**142.1**	**147.8**	**139.3**	**146.9**
P4 Pressure drop (bar)	3.74 bar	3.32 bar	2.40 bar	4.43 bar	4.58 bar
P14 Pressure inlet (bar)	5.96 bar (3 star)	5.92 bar (3 star)	5.90 bar (3 star)	5.89 bar (3 star)	5.79 bar (3 star)
P16 Mass flow rate (kg/s)	0.292 kg/s (3 star)	0.292 kg/s (3 star)	0.289 kg/s (2 star)	0.289 kg/s (2 star)	0.291 kg/s (3 star)
P12 Vapor volume fraction	$2.01*10^{-5}$ (neutral)	$2.01*10^{-5}$ (neutral)	$2.01*10^{-5}$ (neutral)	$2.01*10^{-5}$ (neutral)	$2.01*10^{-5}$ (neutral)

4.2.2 Butterfly valve design results

The main goal was reducing the vapor volume fraction (cavitation) from $2.01*10^{-5}$ to $2.0*10^{-5}$, maximize the mass flow rate and pressure inlet. With pressure inlet at 5.79 bar, pressure drop at 4.58 bar, mass flow rate at 0.291 kg/s, vapor volume fraction at $2.01*10^{-5}$, and flow domain length at 146.9 mm, candidate design 5 meets most of the parameter criteria although it does not meet all the conditions.

4.3 Ball design

Similar design considerations used for the butterfly valve were applied for the ball valve. Figure 20 is the pressure contour showing location of low and high pressure in the ball valve. From those constraints, the following observations are seen: velocity increase in the vena contracta with pressure drop, turbulence and cavitation effects are taking place at the same location [40-50]. Figures 21, 22 and 23, respectively, shows the location of higher velocity, higher turbulence, and vapor volume fraction in the flow occurring in the vena contracta region.

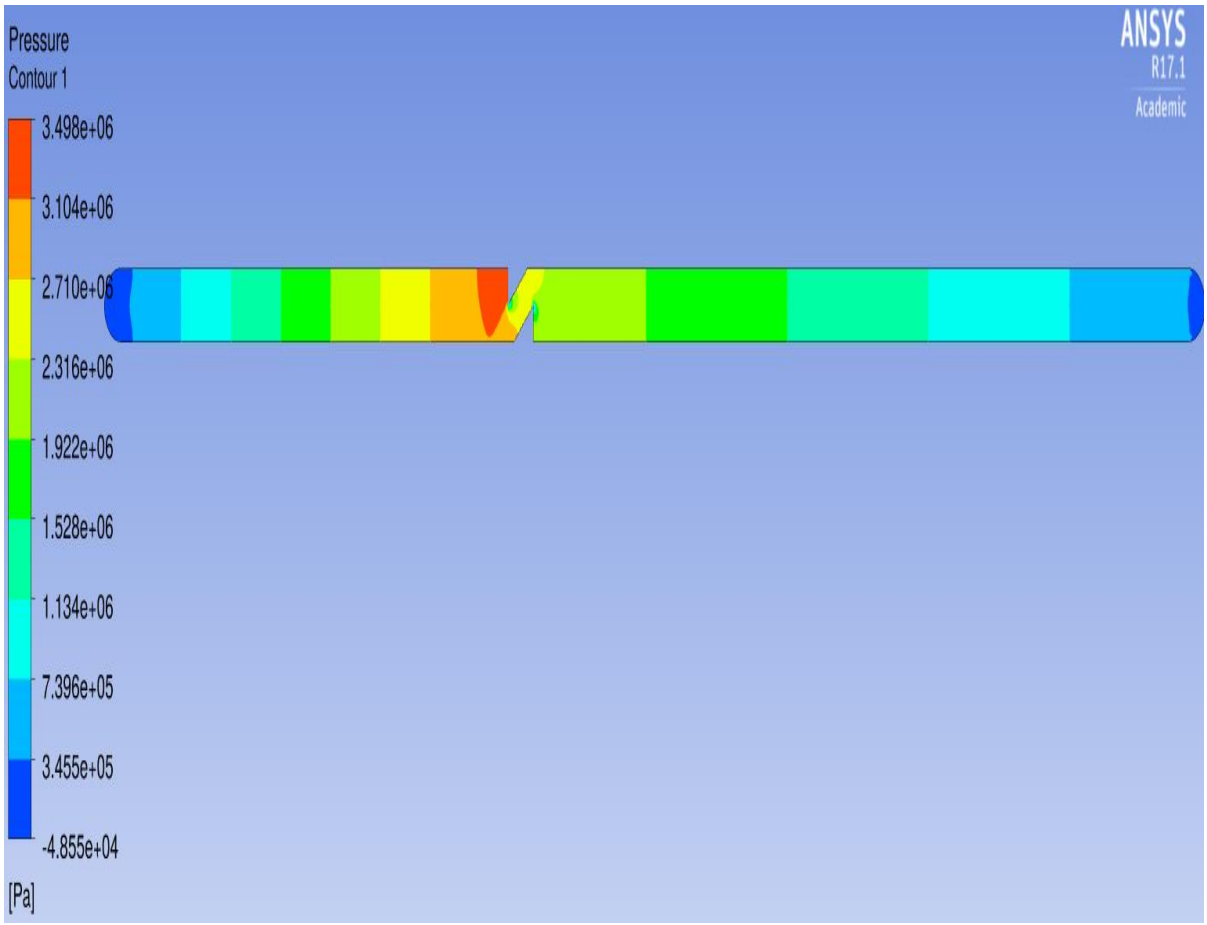

Figure 20: Ball valve pressure inlet contour at 3 bar

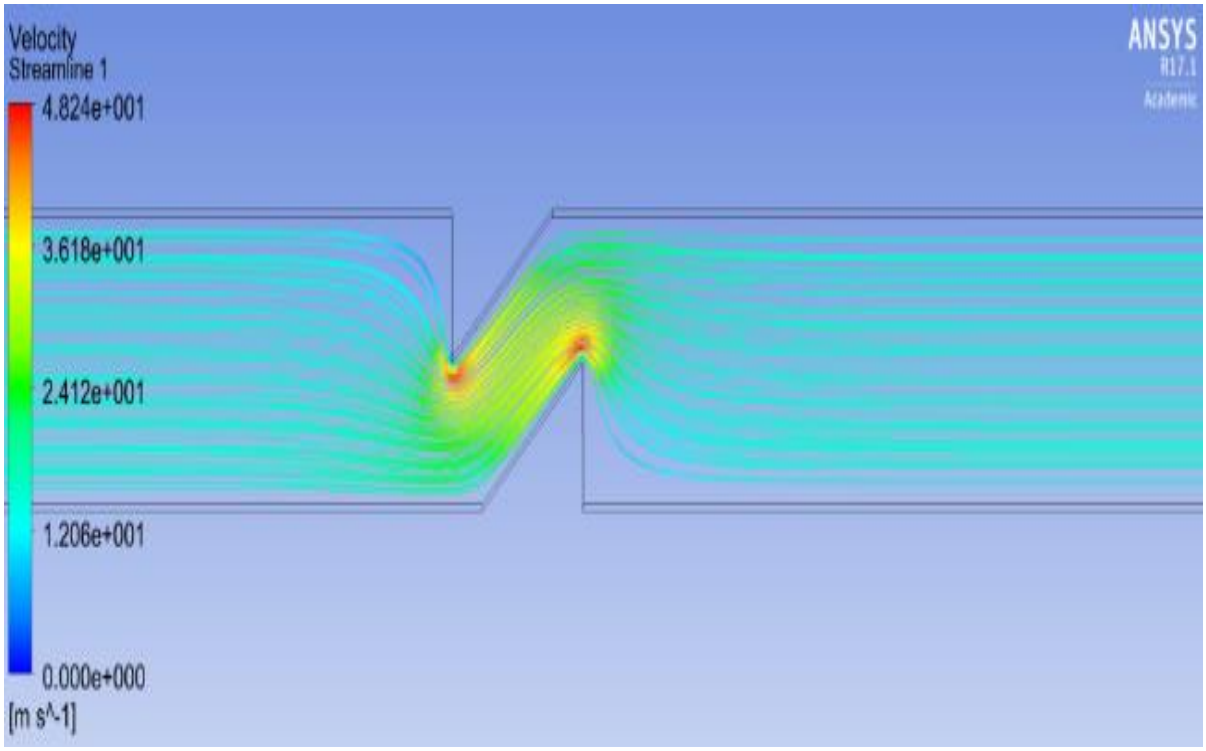

Figure 21: Ball valve velocity streamlines contour in the vena contracta

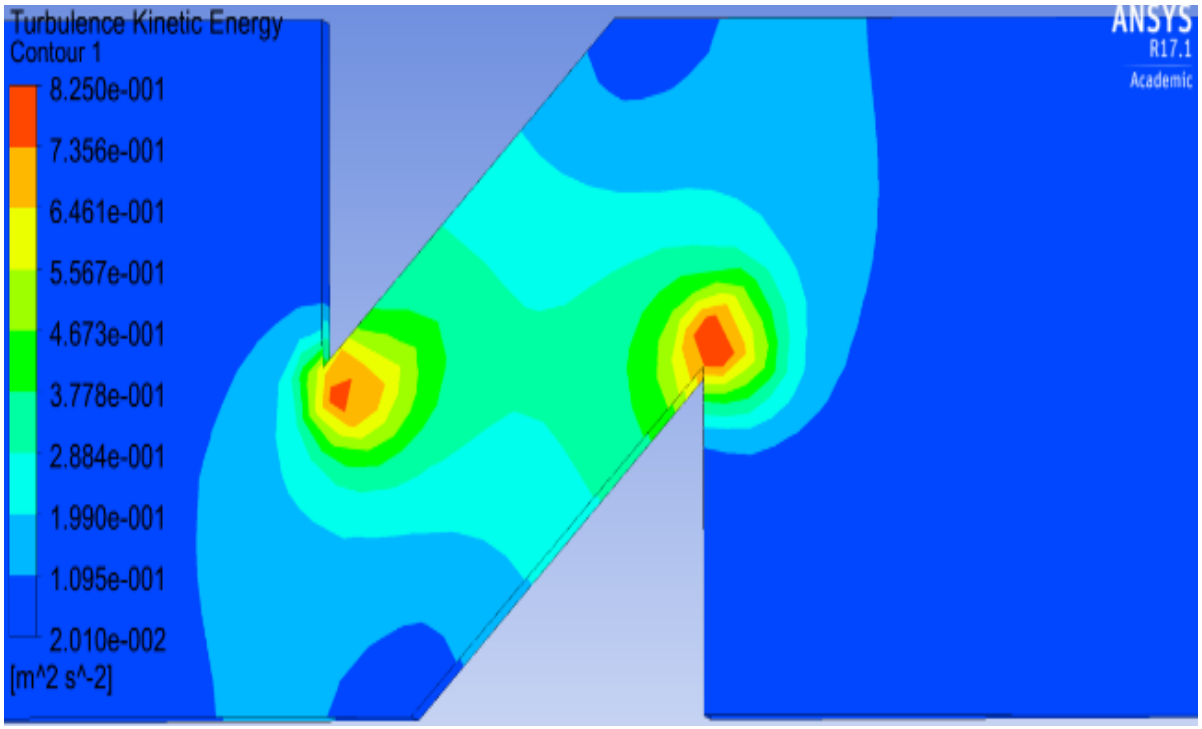

Figure 22: Ball valve turbulent kinetic energy contour at 3 bar

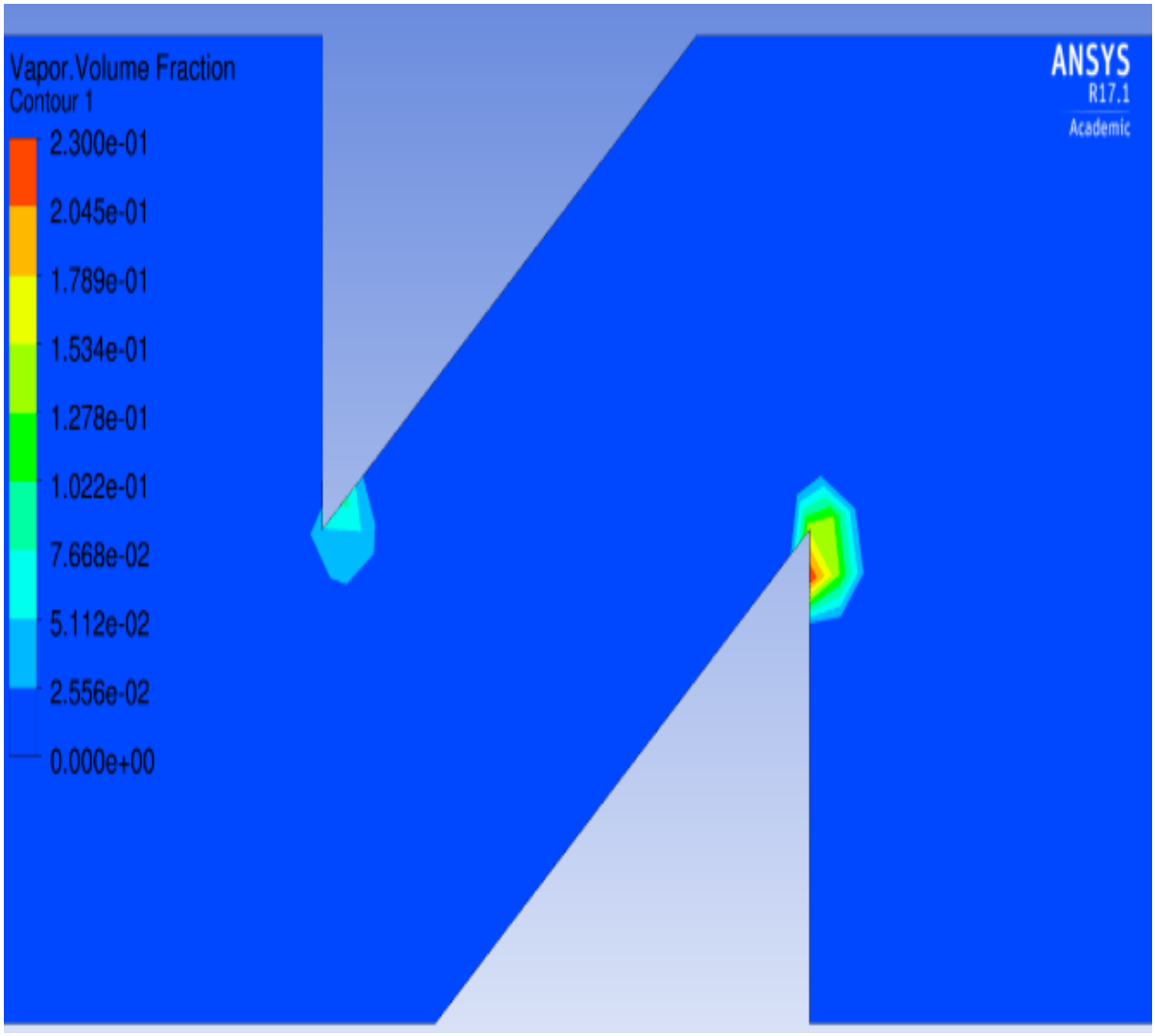

Figure 23: Ball vapor volume fraction (cavitation) region in the flow at 3 bar

4.3.1 Ball valve design set up and optimization

Achieving a decent ball valve design requires accounting for the observed results and design consideration during the DOE. As in the previous design (butterfly), similar steps will be followed for determining sensitive design parameters: design of experiment, response surface, and design optimization. Figure 24 and 25, respectively, show a schematic of the design process and different tabs for each design step used in FLUENT, and the parameters of greater influence in the ball valve design.

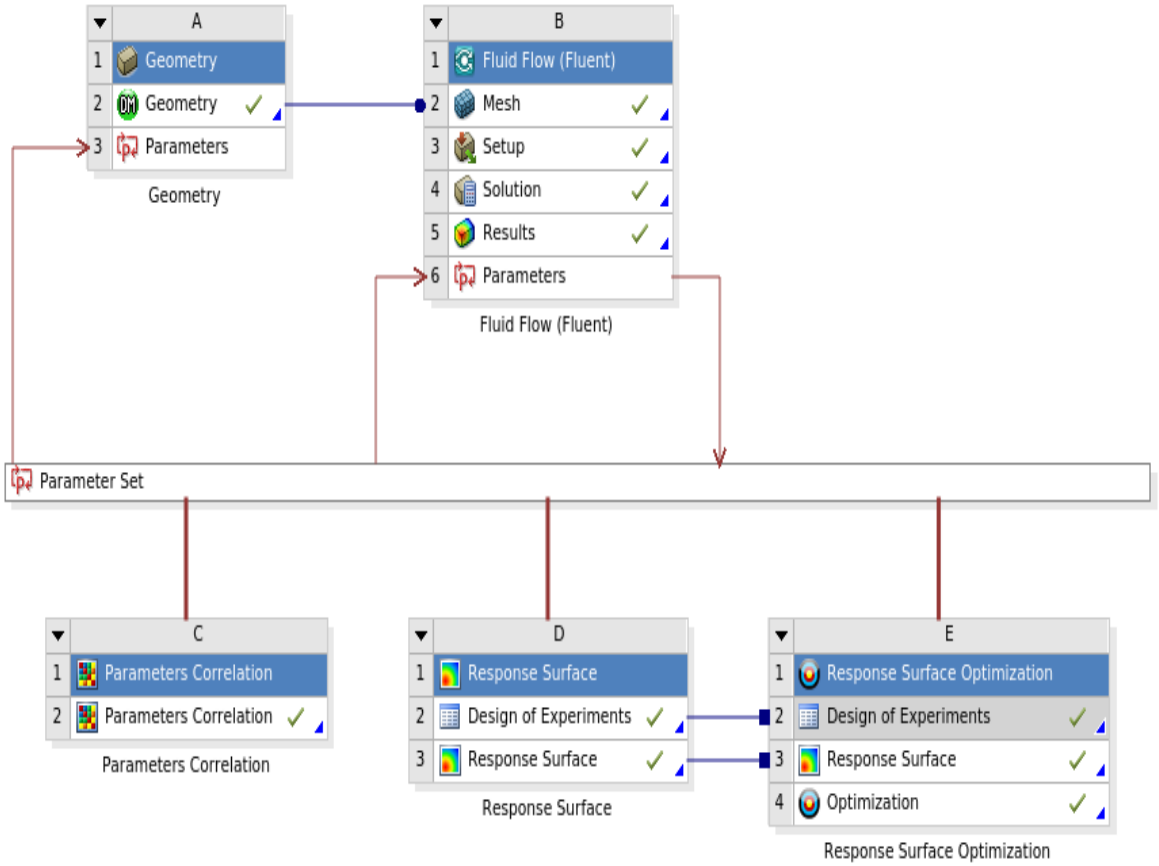

Figure 24: Project schematic to determine parameter correlation, design of experiment (DOE), response surface, and response surface optimization (RSO).

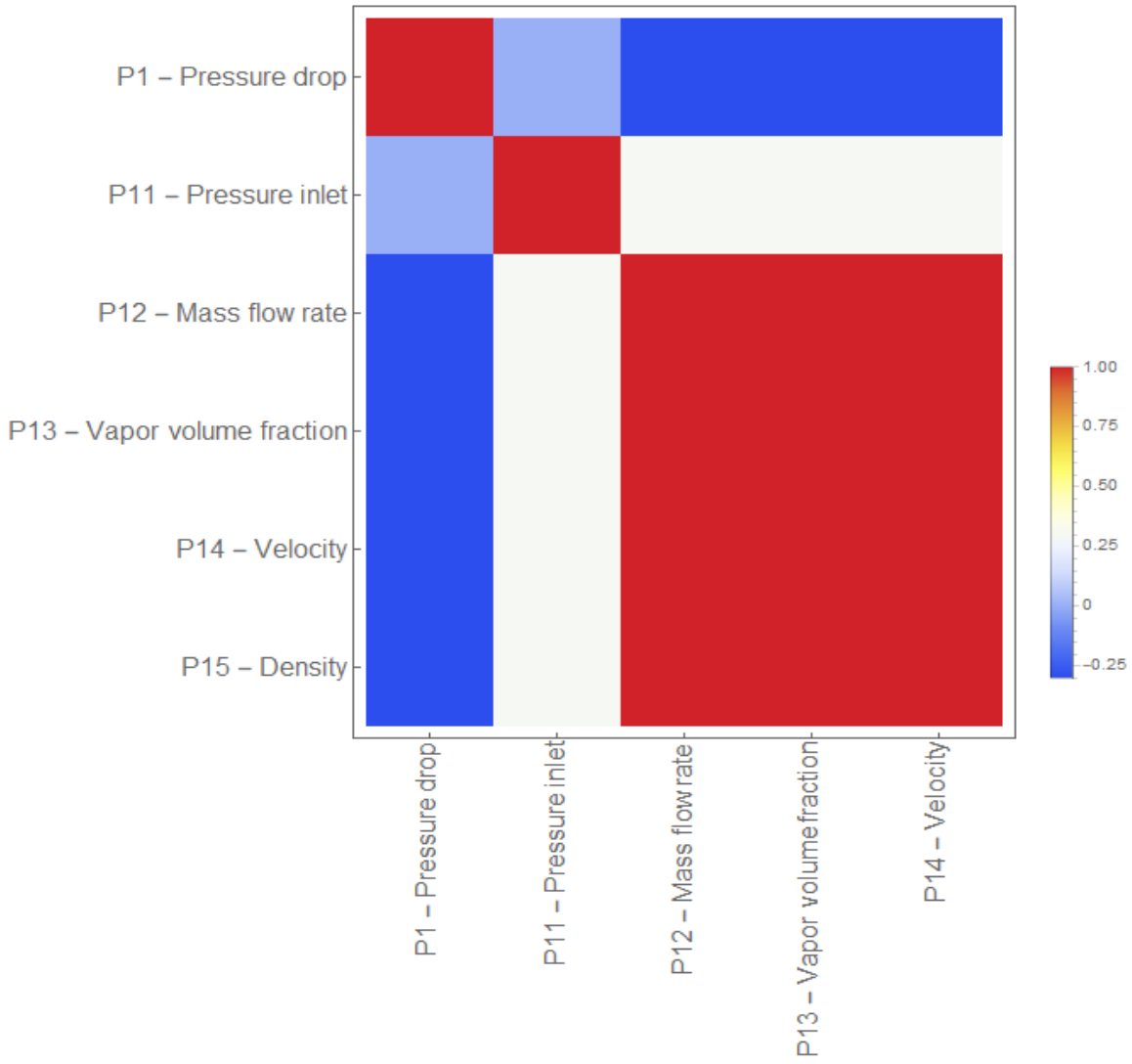

Figure 25: Parameters correlation for ball valve design improvement

As with the previous section (butterfly valve), the design parameters of interest are determined based on input and outputs. The design of experiment is set up, where each parameter selected has a specified bound with a lower and upper value. The parameters of interest in this design are pressure inlet and drop (input) and mass flow rate (output). The DOE is set as follow: Inputs (pressure inlet and drop) and outputs (mass flow rate, density, velocity, and vapor volume fraction). The following outcomes were observed: Pressure drop is directly proportional to mass flow rate, meaning an increase in pressure drop will also

increase the mass flow rate. Pressure inlet is inversely proportional to mass flow rate, meaning an increase in pressure inlet will cause mass flow rate to decrease.

The response surface of the current design is shown in Figure 27. With the current response surface, the ball valve design is poor and requires further optimization. Three parameters (input and output) are selected based on the design objective for optimization. MOGA is used to address design limitations and parameter improvement. Tables 6 and 7, respectively, show the response surface and the response surface optimization with constraints and target.

Table 6: Response surface of ball design

	P12 - Mass flow rate	**P13 - Vapor volume fraction**	**P14 - Velocity**	**P15 - Density**	**Numerical value (star)**
Coefficient of Determination (Best Value = 1)					
Learning Points	0.96	0.96	0.96	0.96	1
Cross-Validation on Learning Points	0	0	0	0	XXX
Root Mean Square Error (Best Value = 0)					
Learning Points		$1*10^{-4}$	$1.28*10^{-6}$	$2*10^{-3}$	---------
Verification Points		$7.73*10^{-5}$	$5.01*10^{-7}$	$9*10^{-4}$	---------
Cross-Validation on Learning Points		$1*10^{-3}$	$7.79*10^{6}$	$7*10^{-3}$	---------
Relative Maximum Absolute Error (Best Value = 0%)					
Learning Points		42.05	42.05	42.05	XXX
Verification Points		7.74	7.74	412.3	Neutral
Cross-Validation on Learning Points		412.3	412.3	412.3	XXX
Relative Average Absolute Error (Best Value = 0%)					
Learning Points		12.5	12.5	12.5	X
Verification Points		7.74	7.74	7.74	Neutral
Cross-Validation on Learning Points		63.6	63.6	63.6	XXX

Table 7: Design parameter optimization from response surface of ball valve design

Optimization study					
Maximize P12	Goal, minimize P12; strict constraint, P12 values < 0.288 kg/s				
Seek P13= $8.464*10^{-5}$	Goal, seek P13				
Minimize P11	Goal, minimize P11				
Optimization method					
MOGA	The MOGA method (Multi-Objective Genetic Algorithm) supports multiple objectives and constraints and aims at finding the global optimum				
Configuration	Generate 1000 samples initially, 100 samples and find 5 candidates in maximum of 20 iterations				
Status	Converged after 1073 evaluations				
Candidate points					
	Candidate point 1	**Candidate point 2**	**Candidate point 3**	**Candidate point 4**	**Candidate point 5**
P16 Pressure drop (bar)	2.00 bar	2.06 bar	2.03 bar	2.01 bar	2.04 bar
P11 Pressure Inlet (bar)	3.00 (3 star)	3.003 (3 star)	3.010 (3 star)	3.011 (3 star)	3.013 (3 star)
P12 Mass flow rate (kg/s)	0.287 (neutral)	0.285 (2 star)	0.286 (1 star)	0.286 (1 star)	0.285 (2 star)
P13 Vapor volume fraction	$8.749*10^{-5}$ (neutral)	$1.039*10^{-5}$ (X)	$9.668*10^{-5}$ (neutral)	$9.363*10^{-5}$ (1 star)	$1.016*10^{-5}$ (neutral)

4.3.2 Ball valve design results

The main goal was reducing the vapor volume fraction (cavitation) from $8.87*10^{-5}$ to $1.01*10^{-5}$, minimize the pressure inlet, and keep the mass flow rate around 0.288 kg/s. With pressure inlet at 3 bar, pressure drop at 2 bar, mass flow rate at 0.287 kg/s and vapor volume fraction at $8.87*10^{-5}$, candidate design 5 meets most of the parameter criteria although it does not meet all the conditions.

5. Conclusions

Ball and butterfly valves opened at 45° open were used to investigate cavitation flow of a mixture model using the commercial software FLUENT. The vapor volume fraction was examined at two different pressures to determine its magnitude and influence on the design. This study evaluated the possibility of obtaining different candidates for an optimal design of both ball and butterfly by using a special feature of the software ANSYS FLUENT. A parameter correlation determined parameters of interest, a design of experiment provided a response surface that was optimized by using the multiple-objective genetic algorithm.

The best candidate for these designs was found although they did not meet all the constraints. Further studies should be devoted to improving the design optimization method and/or process for both valves; finding a candidate that will substantially reduce cavitation, meet all the constraints, before an industrial production scale.

References

[1] B. Lipták, “Cavitation in control valves,” *Control (Chicago, Ill)*, vol. 21, no. 5, pp. 81–82, 2008.

[2] A. Ferrari, “Fluid dynamics of acoustic and hydrodynamic cavitation in hydraulic power systems,” 2017.

[3] Flowserve, “Flowserve Cavitation Control,” pp. 1–20, 2006.

[4] M. J. Chern, C. C. Wang, and C. H. Ma, “Performance test and flow visualization of ball valve,” *Exp. Therm. Fluid Sci.*, vol. 31, no. 6, pp. 505–512, 2007.

[5] K. Tani, Y. Ito, R. Oba, M. Iwasaki, and Y. Hirata, “Studies on Low-Erosion Butterfly Valves,” *JSME Int. J.*, vol. 37, no. 4, pp. 746–751, 1994.

[6] S. Bernad, R. F. Susan-Resiga, S. Muntean, and I. Anton, “Cavitation phenomena in hydraulic valves - Numerical modelling,” *Proc. Rom. Acad. Ser. A*, vol. 8, no. 2, 2007.

[7] G. Brett, M. Riveland, T. C. Jensen, and T. J. Heindel, “Cavitation from a Butterfly Valve: Comparing 3D Simulations to 3D X-Ray Computed Tomography Flow Visualization,” *Jt. fluids Eng. Conf.*, pp. 1–9, 2011.

[8] E. Winklhofer, E. Kull, E. Kelz, and A. Morozov, “Comprehensive hydraulic and flow field documentation in model throttle experiments under cavitation conditions,” *Proc. ILASS-Europe Conf. Zurich*, no. SEPTEMBER, p. 574 – 579, 2001.

[9] E. Christopher, Brennen, *Cavitation and bubble dynamics*, vol. 9, no. 1. 1977.

[10] B. Ji, X. W. Luo, R. E. A. Arndt, X. Peng, and Y. Wu, “International Journal of Multiphase Flow Large Eddy Simulation and theoretical investigations of the transient cavitating vortical flow structure around a NACA66 hydrofoil,” vol. 68, pp. 121–134, 2015.

[11] S. I. Bernad and R. Susan-Resiga, “Numerical model for cavitational flow in hydraulic poppet valves,” *Model. Simul. Eng.*, vol. 2012, 2012.

[12] W. Wienken, J. Stiller, and A. Keller, “A method to predict cavitation inception using large-eddy simulation and its application to the flow past a square cylinder,” *J. Fluids Eng. Asme*, vol. 128, no. 2, pp. 316–325, 2006.

[13] a Fluent, “Ansys Fluent 15.0 Tutorial Guide,” Ansys INC, vol. 15317, no. November, pp. 891–920, 2013

[14] ANSYS, “ANSYS Fluent Theory Guide,” vol. 15317, no. November, p. 514, 2013.

[15] T. D. Canonsburg, “ANSYS Fluent Meshing User’s Guide,” vol. 15317, no. November, pp. 724–746, 2013.

[16] J. D. Anderson Jr., “Computational fluid dynamics- The basics with applications,” McGraw-Hill, Inc., vol. 27, no. 6. pp. 1661–71, 1995.

[17] M. A. R. Cunha and H. F. V. Nova, “Cavitation modeling of a centrifugal pump impeller,” *22nd Int. Congr. Mech. Eng.*, vol. m, no. November, pp. 1633–1644, 2013.

[18] B. Ji, X. Luo, X. Peng, Y. Wu, and H. Xu, “International Journal of Multiphase Flow Numerical analysis of cavitation evolution and excited pressure fluctuation around a propeller in non-uniform wake,” *Int. J. Multiphase. FLOW*, vol. 43, pp. 13–21, 2012.

[19] M. S. Plesset and R. B. Chapman, “Collapse of an initially spherical Vapor Cavity in the Neighborhood of a solid Boundary,” J. Fluid Mech., vol. 47, no. 2, pp. 283–290, 1971.

[20] E. A. Brujan, G. S. Keen, A. Vogel, and J. R. Blake, “The final stage of the collapse of a cavitation bubble close to a rigid boundary,” *Phys. Fluids*, vol. 14, no. 1, pp. 85–92, 2002.

[21] P. G.-A. and J. A.-V. G. Palau-Salvador, “Introduction,” *Spanish J. Agric. Res.*, vol. 5, no. 4, pp. 460–469, 2007.

[22] A. Iannetti, M. T. Stickland, and W. M. Dempster, “A CFD and experimental study on cavitation in positive displacement pump: benefits and drawbacks of the ‘full’ cavitation model,” *Eng. Appl. Computational. Fluid Mech.*, vol. 10, no. 1, pp. 57–71, 2015.

[23] A. Karimi and J. L. Martin, “Cavitation erosion of materials,” *Int. Mater. Rev.*, vol. 31, no. 1, pp. 1–26, 1986.

[24] A. Del Toro, “Computational Fluid Dynamics Analysis of Butterfly Valve. Performance factors.” 2012.

[25] M. Morgut and E. Nobile, “Influence of the Mass Transfer Model on the Numerical Prediction of the Cavitating flow around a Marine Propeller,” *Second Int. Symposium. Mar. Propulsors smp’11*, no. June, pp. 1–8, 2011.

[26] A. Adamkowski and M. Lewandowski, “Consideration of the cavitation characteristics of shut-off valves in numerical modeling of hydraulic transients in pipelines with column separation,” *Procedia Eng.*, vol. 70, pp. 1027–1036, 2014.

27] Z. Yao, L. Xian-Wu, L. Shu-Hong, W. Yu-Lin, and X. Hong-Yuan, “A Thermodynamic Cavitation Model for Cavitating Flow Simulation in a Wide Range of Water Temperatures,” *Chinese Phys. Lett.*, vol. 27, no. 1, p. 16401, 2010.

[28] M. Morgut and E. Nobile, “Numerical predictions of the cavitating and non-cavitating flow around the model scale propeller pptc,” *... Work. Cavitation Propeller*, no. June, 2011.

[29] T. D. Canonsburg, “Design Exploration User’s Guide,” vol. 15317, no. November, pp. 724–746, 2013. 2

[30] D. Odhiambo and H. Soyama, “Cavitation shotless peening for improvement of fatigue strength of carbonized steel,” *Int. J. Fatigue*, vol. 25, no. 9–11, pp. 1217–1222, 2003.

[31] Z. Li and T. Van Terwisga, “On the Capability of Multiphase RANS Codes to Predict Cavitation Erosion,” *Second Int. Symp. Mar. Propulsors*, no. June, 2011.

[32] S. Rammohan and S. Kumaraswamy, “Numerical prediction and experimental verification of cavitation in butterfly valves,” *Symp. A Q. J. Mod. Foreign Lit.*, no. September, pp. 8–13, 2006.

[33] D. Rossinelli, P. Koumoutsakos, B. Hejazialhosseini, P. Hadjidoukas, C. Bekas, a. Curioni, a. Bertsch, S. Futral, S. J. Schmidt, and N. a. Adams, “11 PFLOP/s simulations of cloud cavitation collapse,” *Proc. Int. Conf. High Perform. Comput. Networking, Storage Anal. - SC ’13*, pp. 1–13, 2013.

[34] M. Turesson, “Dynamic simulation of check valve using CFD and evaluation of check valve model in RELAP5,” 2011.

[35] G. H. Schneer and J. Sauer, “Physical and Numerical modelling of unsteady cavitation dynamics.” *Int. Conf. Multiphase. Flow*, vol. 11, no. 4, pp. 391–400, 2001.

[36] E. Koyunbaba, “Graduate School Of Natural And Applied Sciences Computational Fluid Dynamics Application For Determining Flow Computational Fluid Dynamics Application For Determining Flow,” 2008.

[37] Val-Matic Valve And Manufacturing Corp, “Cavitation in Valves,” *Val-Matic*, no. 630, pp. 1–5, 2011.

[38] Y. Xu, Y. Chen, J. He, and H. Yan, “Detection of Cavitation in a Venturi Injector With a Combined Method of Strain Gauges and Numerical Simulation,” *J. Fluids Eng.*, vol. 136, no. 8, p. 81302, 2014.

[39] W. Li, “Validating Full Cavitation Model With an Experimental Centrifugal Pump,” *TASK Q.*, vol. 18, no. 1, pp. 81–100, 2014.

[40] R. Bosch and G. Bosch, “Experimental and CFD technology for preventive reduction of diesel engine emissions caused by cavitation erosion,” 2002.

[41] S. Rammohan and S. Kumaraswamy, “Numerical prediction and experimental verification of cavitation in butterfly valves,” *Symp. A Q. J. Mod. Foreign Lit.*, no. September, pp. 8–13, 2006.

[42] H. Soyama, K. Saito, and M. Saka, “Improvement of fatigue strength of aluminum alloy by cavitation shotless peening,” *J. Eng. Mater. Technol. Asme*, vol. 124, no. 2, pp. 135–139, 2002.

[43] D.-Q. Li, M. Grekula, and P. Lindell, “A modified SST k-\omega turbulence model to predict the steady and unsteady sheet cavitation on 2D and 3D hydrofoils, ” *Int. Symp. Cavitation*, no. 107, pp. 1–13, 2009.

[44] B. J. Solomon, “Engineering Model to Calculate Mass Flow Rate of a Two-Phase Saturated Fluid Through An Injector Orifice,” 2011.

[45] B. S. Waxman, J. E. Zimmerman, B. J. Cantwell, and N. Ames, “Mass Flow Rate and Isolation Characteristics of Injectors for Use with Self-Pressurizing Oxidizers in Hybrid Rockets,” pp. 1–32, 2013.

[46] D. Q. J. D. Kljxr and K. D. Xh, “Numerical Simulation of Fluid Flow inside the Valve,” vol. 23, no. 1, pp. 543–550, 2011

[47] D. Rossinelli, P. Koumoutsakos, B. Hejazialhosseini, P. Hadjidoukas, C. Bekas, a. Curioni, a. Bertsch, S. Futral, S. J. Schmidt, and N. a. Adams, “11 PFLOP/s simulations of cloud cavitation collapse,” *Proc. Int. Conf. High Perform. Comput. Networking, Storage Anal. - SC ’13*, pp. 1–13, 2013.

[48] J. Necker and T. Aschenbrenner, “Model test and CFD calculation of a cavitating bulb turbine,” *IOP Conf. Ser. Earth Environ. Sci.*, vol. 12, p. 12064, 2010.

[49] Kounbaba, E., “Computational Fluid Dynamics application for characteristics of valves,” 2008.

[50] H. Li, F. J. Kelecy, A. Egelja-maruszewski, and S. A. Vasquez, “Paper No . IMECE2008-67450 Advanced computational modeling of steady and unsteady,” pp. 1–11, 2008.

CHAPTER 3. TECHNO-ECONOMIC ANALYSIS OF TRANSPORTATION FUELS FROM PINEWOOD VIA HYDROTHERMAL LIQUEFACTION

Nzombo, D., Li W., Brown R., Wright M. manuscript in preparation

Abstract

The purpose of this study is to develop a techno-economic analysis model to evaluate the economic feasibility of transportation fuel production by solvent liquefaction (SL) of pine wood in a novel hydrocarbon solvent, followed by hydroprocessing of medium wood oil (MWO) and heavy wood oil (HWO). A 2000 dry tonne per day biorefinery produces 364 dam^3 of MWO and 76 dam^3 per year. The total project investment is estimated at $331 M and the annual operating cost is $110 M. The minimum fuel selling price (MFSP) is $0.94/gallon assuming a 10% internal rate of return and a 30-year plant life. A sensitivity analysis shows that the MFSP is most sensitive to the product fuel yield showing the respective importance of SL conversion performance. Feedstock cost also has a strong and significant influence on the MFSP, which respectively varied between $0.80/gallon to $1.19/gallon for feedstock cost of $33 and $132 dry $tonne^{-1}$.

1. Introduction

Greenhouse gases (GHG) have contributed to global warming and raised environmental concerns over energy use, and prompted renewed interest in clean energy resources such as biomass. Biomass is defined as biodegradable and renewable organic matter. Clean and renewable transportation fuels based on biomass have been getting more attention as an alternative to fossil fuels. The Energy Independence and Security Act (EISA) of 2007 require blending biofuels for transportation purposes under the revised Renewable Fuel Standard (RFS2). This study will evaluate the techno-economic cost of using Pinewood as biomass feedstock with a hydrocarbon solvent and its conversion into transportation fuels. Pinewood has great potential as a biomass resource for the production of biofuels with reduced land use and low CO_2 emissions [1, 2].

Pinewood presents a great advantage as it is largely available in the southeastern part of the United States (US), covering a land area of 13 million ha, and could be sustainably used for bio-oil production [3, 4]. Pinewood is essentially composed of cellulose, lignin, and extractives [5]. Their unique composition makes them appropriate for several applications.

Pinewood can be employed in different thermochemical pathways such as catalytic liquefaction, gasification and fast pyrolysis [2, 7-8]. However, there are some disadvantages of using pyrolysis liquid for chemical and fuel applications. These include its high moisture content (15-30 wt. %), oxygen content (35-40 wt. %), and a low heating value compared to fossil fuels [2, 8]. The disadvantage of gasification is tar formation, which reduces the efficiency of gas production and restricts equipment operation [8]. With direct liquefaction, a simple direct conversion of biomass to liquid fuel results in high liquid yields [9]. Direct liquefaction is a process that includes fast pyrolysis and high-pressure SL [9]. Bio-oil from

the SL process results in lower oxygen content (10-20 wt. %) and a higher heating value of 35 MJ/kg compared to fast pyrolysis, which has twice as much oxygen content (about 40 %) and lower heating value (16-19 MJ/kg) [9]. In rural and urban areas, wood is often burned in cooking, heating, fireplace, campfire, and waste disposal [6]. The volatiles, which accounts for as much as 82.6 wt. % of the whole pinewood [11], could be used for biofuel production based on its hydrogen and carbon content [8].

Past studies clearly identify different applications for pinewood including char and biofuel [2, 12] via pyrolysis and gasification. Pinewood could be converted into liquid fuels compatible with the existing transportation fuel infrastructure [14, 15]. However, the costs of producing transportation fuels from petroleum remain too low for biofuels to be economically competitive in US markets. Thus, technologies that can recover higher valued fuels and chemicals need to be identified to improve the profitability of biorefineries.

Phenolic monomers are lignin compounds with large oxygen content [16]. Due to its large oxygen content, phenolic monomers require hydrodeoxygenation to convert into regular and conventional transportation alkane fuels [16, 17]. Phenolic are considered an important compound for bio-oil, and hydrodeoxygenation is a crucial process for its upgrade into bio-oil [18, 19]; generally, the upgrade is completed by using a catalyst [16]. They can also be used differently in solvent liquefaction. Phenolic monomers would be mixed with a hydrocarbon solvent to help convert pinewood into liquid [11] in the front process and will be followed by the hydroprocessing and upgrading of heavy bio-oil products into gasoline and diesel fuels [11].

Various thermochemical technologies such as gasification, catalytic and fast pyrolysis, and solvent liquefaction (SL) [15, 20] can convert biomass into biofuels and

chemicals. Pyrolysis and gasification are not ideal for producing phenolic monomers in addition to bio-oil. SL offers the opportunity of producing phenolic monomers by using a hydrocarbon solvent [11]. SL involves processing biomass in pressurized water temperature between 250 and 550°C, and pressures of 5-50 bar. SL products include a heavy or crude oil phase, an aqueous fraction, and a gaseous fraction [21, 22]. The crude oil produced by SL is often called bio-crude, which has a relatively high heating value (>30 MJ Kg^{-1}) [9, 22]. SL has been employed to process lignocellulosic biomass in the presence of a catalyst and/or solvents in various studies [23, 24].

SL, compared to other thermochemical technologies, has the advantage of producing bio-crude with lower oxygen content and higher heating value. These bio-crude characteristics make it more suitable for upgrading in crude-oil refineries [2, 8]. SL can effectively utilize biomass feedstock with high moisture content, which avoids the energy consumption for biomass drying [9]. Additionally, SL may not result in water evaporation, as in gasification and pyrolysis. Instead, SL can maintain hot compressed water in the liquid phase [9]. Biomass SL has only been demonstrated and studied up on the pilot scale, unlike gasification and pyrolysis whose systems have been commercially available [25-26]. However, a substantial downside of SL is the severe operating conditions required (high temperature and high pressure) incurring high investment and operating costs [27-28].

To our knowledge, there is very limited number of public studies that have investigated the techno-economic analysis (TEA) feasibility of biofuel production from pinewood. Liquefaction and SL were examined as potential routes to convert pinewood into bio-crude [9], and the bio-crude could be hydroprocessed and upgraded to gasoline and diesel

fuel. Previous research has shown that SL has a better energy balance compared to slow pyrolysis [6, 9, 22].

In this study, a TEA is conducted to determine the potential for producing transportation liquid fuels from pinewood and hydrocarbon solvent via SL to obtain Medium Wood Oil (MWO) and Heavy Wood Oil (HWO). A commercial-scale 2000 dry tonne per day SL and a hydroprocessing facility is modeled to estimate the total project investment and annual operating costs. The process model assumes that the facility (plant) is mature, and all the technical challenges have been overcome and the materials are commercially available. The potential commercialization is conditioned by the competitiveness of the minimum fuel selling price (MFSP) relative to market alternatives. The MFSP is determined based on a 10% internal rate of return (IRR) and a 30 year lifetime of the facility.

2. Materials and Methods

The TEA uses chemical process modeling and economic cost analysis to determine the process profitability. Aspen Plus™ was the software employed in this study for process modeling. Cost estimation and purchase of equipment such as compressors, heat exchangers, and pumps were estimated in Aspen Process Economic Analyzer and from public literature. Cost estimation and purchase of engineered equipment such as the SL reactor and hydrogen plant are projected based on a power law frequently employed with a scaling factor of 0.6 for chemical processing equipment [28-30], which is represented by:

$$Cost_{new} = Cost_{base}\left(\frac{Capacity_{new}}{Capacity_{base}}\right)^{scaling\ factor} \quad (1)$$

The return on investment is estimated with a 30 year discounted cash flow rate of return (DCFROR) spreadsheet. There are five major assumptions made in this study: (1) Plant capacity is 2000 dry tonne per day of pinewood, (2) the feedstock contains 82.6 % of

volatiles, (3) liquid effluent and recycled medium wood oil from SL reactor are directed in overhead separation unit, then to a phase separator, and to a waste water treatment plant, (4) dry char and non-condensable gases (NCG) are used to heat the NCG stream for heating and the liquefaction reactor and fuel gas for the furnace, and (5) the cost analysis represents an n^{th} plant design, meaning all the major technical obstacles have been overcome and required equipment is commercially available.

2.1 Process modeling

The chemical process model has 4 areas: Solvent liquefaction (SL), hydroprocessing, product refining, and a combined heat and power (CHP) plant. Figures 1 and 2, respectively, show a simplified and a detailed version of the flow diagram of SL, and product refining processes. As shown, the hydrocarbon solvent and pinewood feedstock enter the liquefaction section along with a recycled stream of MWO and solvent. SL products leave the liquefaction section and are separated into streams of NCG, biochar, LWO and acids, and HWO and MWO (bio-crude). The HWO and MWO stream are stabilized and stored before shipping for upgrading at an external facility such as a refinery. The process generates steam on-site for liquefaction by combusting the NCG and off-gas. Requisite hydrogen is generated via steam reforming of LWO and acids and supplemental natural gas. The hydrogen is employed to stabilize the bio-crude product. Waste handling and disposal were not included in the model. SL wastewater will be treated by a third party at a fixed price per unit volume ($\$0.89\ m^{-3}$) [31], and solid waste can be disposed at a fixed price per unit mass ($\$36.98\ tonne^{-1}$) [32].

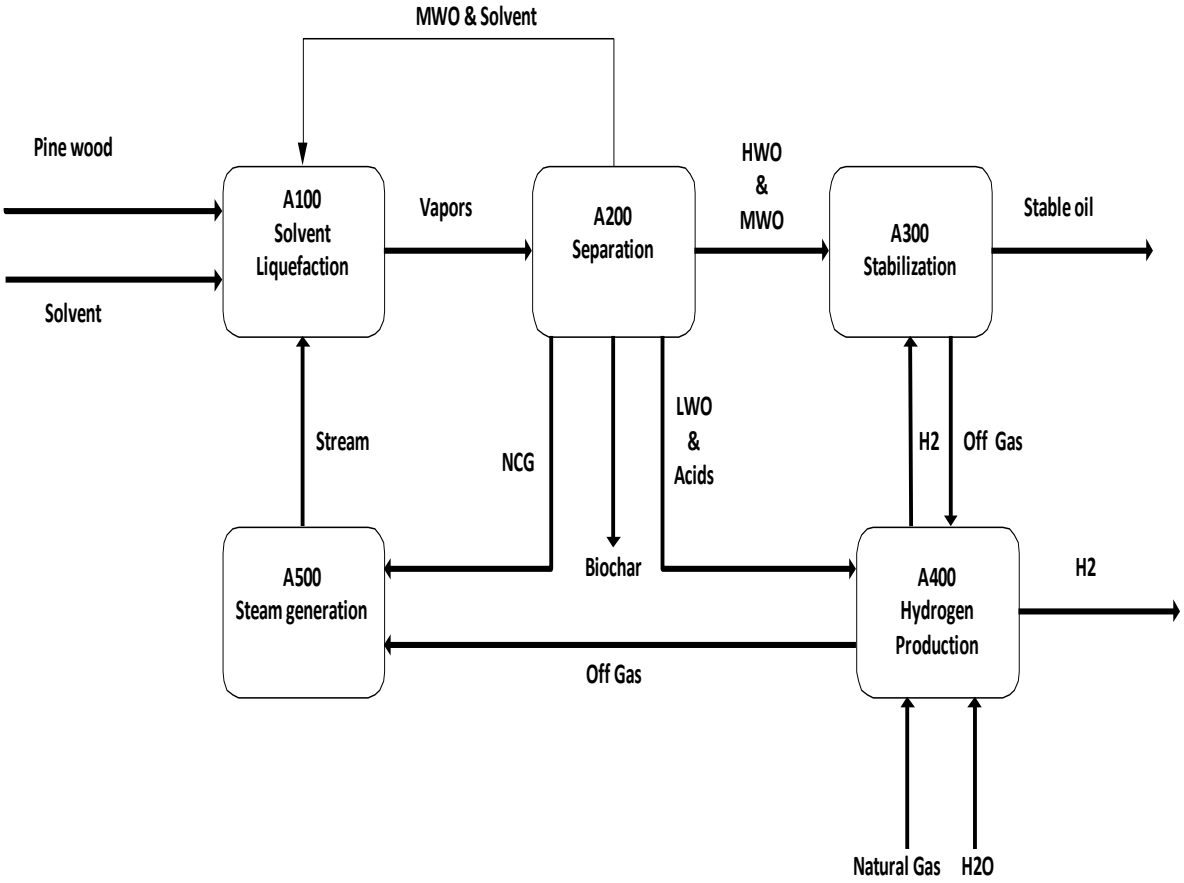

Figure 1: Schematic of the pinewood solvent liquefaction process for gasoline and diesel

2.1.1 Biomass feedstock

The feedstock was composed of 0.63 centimeter size particles. The moisture content is about 5 wt. %, and volatiles accounts for 82.6 wt. % of the pinewood [11]. Table 1 shows the elemental composition of pinewood in atomic mass fraction (AF) of dry material and mass fraction (MF) of dry feed.

Table 1: Pinewood proximate and ultimate analysis

Proximate Analysis	(wt. %)	Ultimate Analysis	(wt. %, AF/MF)
Moisture	~5	C	52.0
Volatiles (MF)	82.6	H	5.37
Fixed Carbon (MF)	13.3	O	42.6
Ash (MF)	0.55	N	0.05
----------	----------	S	0.02

Biomass availability in the US is estimated to be around 370 million to 1.3 billion dry tons/year of biomass, which could theoretically replace about 60 billion gallons of the US annual petroleum consumption [33]. Woody biomass is largely available and estimated to account for about 39% (368 million tons) of the total biomass in the US [4]. Its abundance makes it one of the most affordable feedstocks on the market for biofuel production [33]. Due to its use for other applications, a large amount of leftover and wood waste is available [3, 4, 33]. Resulting in lower cost and availability of pinewood as a feedstock for SL.

2.2 Solvent liquefaction process

2.2.1 Conversion

First, 7,000 tonne/day of solvent, composed of 75 wt. % of heavy aromatic solvent (HAS) and 25 wt. % of hydrogenated light cycle oil (HLCO) are co-fed to the extruder (reactor) with 2,000 tonne/day dry biomass. The mixture is liquefied at 400°C and 41 bar in the extruder. The resulting mixture of gas/liquid/solids is then fed to the flash separator unit (SEP-1). The mixture is cooled from 400°C to 288°C under constant pressure during its transition between the extruder and flash separator. Meanwhile, the heavy liquid products and bio-char remain in the liquid pool in SEP-1, while the lighter liquid products and non-condensable gases are sent to the overheads section.

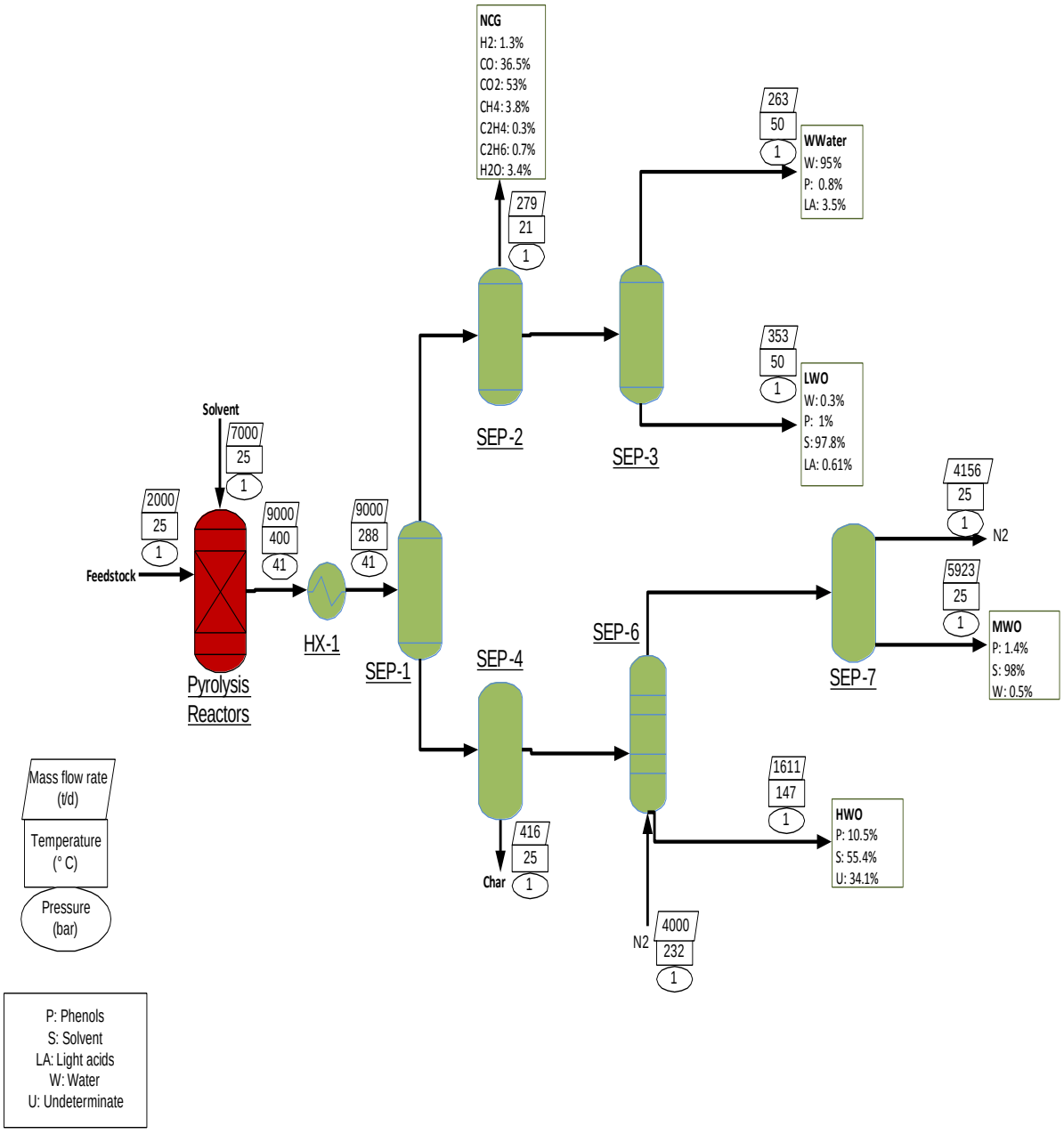

Figure 2: Process flow diagram for pinewood solvent liquefaction and product refining.

SEP-2 acts as a second flash separator where a single liquid phase is collected and the NCG leave as the overhead. After leaving SEP-1, the lighter liquid products and NCG are cooled down close to 21° C before entering SEP-2. The NCG exit SEP-2 through a valve where its pressure is reduced from 41 bar to 1 bar. The liquid products in SEP-2 leave the

unit through a valve at the bottom into another flash separator (SEP-3). After going through the valve, the pressure of the liquid drops from 41 bar to 1 bar and temperature from 33° C to nearly 25° C. The resulting liquid products are an organic phase and an aqueous phase.

The heavier liquid products and solids are transferred from SEP-1 into a mixing tank through batch valves. This results in a pressure reduction of the heavy liquid products/solids to 1 bar, while dissolved gases are released during this process and combined with the overheads gas products. During the transfer from SEP-1 to the mixing tank, the temperature of the mixture drops to 21 °C. The liquid and solids products are removed from the SEP-2 using a pump and filter (F-C). The liquid product is then held in a collection vessel (SEP-4) at 50 °C and 1 bar.

The liquid product from the filtration unit is pumped through a heat exchanger and heated to a temperature of 147 °C. The heated heavy liquid products are then fed to a stripping column (SEP-6) operating at 232 °C and 1 bar. The stripping gas used is N_2 at a flow rate of 4,000 tonne/day and a temperature of 232 °C. The lighter components exit the stripping column overhead and are cooled down to almost 25 °C. They are then collected in another flash separator (SEP-7), and the non-condensable gases (mainly N_2) exit through the top of SEP-7. The heavy products are collected from the bottom of SEP-6. The process conditions and functions are summarized in Table 2.

Table 2: Pinewood solvent SL process key operating units and conditions

	SL Reactor		Overheads Separator		Filtration		Fractionation
Unit	EX-1	SEP-1	SEP-2	SEP-3	SEP-4	SEP-6	SEP-7
Function	Reactor	Flash	Flash	Flash	------	-------	--------
Temperature (°C)	400	288	21	50	25	232	25
Pressure (bar)	41	41	41	1	1	1	1

The aqueous phase is to be sent to a water treatment facility. Minor compounds in this stream include light acids and lighter phenolic products. The gaseous phase, which consists of NCG (mainly stripping N2) and light products, is sent to the combustor area to be combusted for supply process heat. The bio-crude is sent to the hydroprocessing process to be deoxygenated via hydrotreating using a cobalt molybdenum catalysts [29]. The medium wood oil (MWO) is recycled to the front of the system, minimizing fresh solvent input. Table 3 shows the main components of the key process streams.

Table 3: Key process streams and concentration of phenols (P), Light Acids (LA), Water (W), Undetermined (U), and solvent

	Conversion			Overheads		Filtration	Fractionation		Extra
	Stream	Biomass	Solvent	LWO	Aqueous phase	S	HWO	MWO	NCG
	Mass Flow (tonne/day)	0.0545 dry/0.00115 H2O	37.9 (75 wt. % HAS/25 wt. % HLCO)	0.430	2.68	2.08	10.7	32.1	1.56
Component Concentration (Wt. %)	P	—	—	2.48	3.05	—	10.7	1.93	—
	LA	—	—	0.777	8.12	—	10.9	0.175	—
	W	—	—	0.822	82.3	—	0.0433	0.862	—
	U	—	—	—	—	—	0.796	—	—
	Solvent		100	95.9	6.53	—	37.3	97.0	—

2.2.2 Combined heat and power plant

In this area, off-gas streams are combined and combusted to recover process heat. Flue gas from the combustor is used to preheat air fed to the combustor and heat exchanger.

The primary heat consumers in this process are the SL reactor, steam reformer, and natural gas heater. Superheated steam (449° C, 6 bar) [24] is split into 2 streams. The first stream provides dedicated heat to the SL reactor. The second provides both heat and power by going through a multistage turbine and power generator. Steam is extracted at three different conditions for use in this process. High-pressure steam at 4.2 bar, medium pressure steam at 1.1 bar and low-pressure steam at 0.6 bar [30] are also extracted. Part of the high-pressure steam is used to preheat the boiler feed water. Low-pressure steam is sent to the flash separator to dissolve gases from the boiler [24]. In the final stage of the turbine, the expanded steam is cooled and condensed to 0.01 bar and 46° C [35]. Boiler blowdown is assumed to be 3% of the steam production [24]. The generated electricity is supplied to users of the plant. Purchased electricity supplies the remainder of the plant power demand.

3. Economic analysis

A process model is built in Aspen Plus to obtain material and energy balance of the pinewood SL pathway. Process equipment units are sized based on the material, energy balances, and operating costs. Purchased costs of common equipment such as pumps, compressors, and vessels are estimated using Aspen Plus™. The cost of complex equipment such as reactors and distillation columns are estimated by scaling up publicly available data for similar equipment [29, 36]. Once the Total Purchased Equipment Cost (TPEC) is obtained, Fixed Capital Investment (FCI) and Total Project Investment (TPI) can be determined from Peters and Timmerhaus [34, 37] factors. All the parameters used for the estimation of FCI and TPI from TPEC are listed in Table 4. The results were used as input information into a modified DCFROR analysis spreadsheet to calculate the MFSP.

Table 4: Total project investment cost factors (all results in 2011 dollars) [35]

Direct cost	M$
Total purchased equipment cost (TPEC)	65
Purchased equipment installation	26
Instrumentation and controls (installed)	16
Piping (installed)	16
Electrical systems (installed)	7
Buildings (including services)	18
Yard improvements	9
Service facilities (installed)	39
Total installed cost (TIC)	196
Indirect costs	
Engineering and supervision	21
Construction expenses	22
Legal expenses	4
Contractor's fee	15
Contingency	24
Total indirect cost	86
Fixed capital investment (TIC + indirect plant costs)	282
Working capital (15% of total capital investment)	49
Total project investment (Fixed capital investment + working capital)	331

Table 5 shows the main assumptions of the economic analysis. The plant life is 30 years, and it operates for 7884 hours per year. The facility is financed through 100% equity. The general and steam plant depreciation follows a double declining balance (DDB) schedule with a 7-year period for the general plant and 20 year period for the steam plant. The project investment schedule during construction has 32%, 60%, and 8% spent over the course of 3 years [35]. Once completed, the facility startup time is half a year. During the startup time, the facility generates 50% of its full capacity revenue but incurs 75% of variable and 100% of fixed costs. The internal rate of return (IRR) is set at 10%, and the income tax rate is 39%. A standard 15% contingency factor was included to consider any unexpected and unforeseen expenses during the startup period [29, 39].

Table 5: Major biorefinery economic analysis assumptions [28]

Plant life (years)	30
Operating hours per year	7884
Equity	100%
General/Steam plant depreciation	double declining balance (DDB)
Depreciation period (years)	
General plant	7
Steam/electricity	20
Construction period (years)	2.5
Fraction of investment in year -3(%)	8.00
Fraction of investment in year -2(%)	60.00
Fraction of investment in year -1(%)	32.00
Start-up time (years)	0.5
Revenues (% of normal)	50%
Variable costs (% of normal)	75%
Fixed cost (% of normal)	100%
Internal Rate of Return	10%
Income tax rate	39%

Annual operating costs include the cost for feedstock, natural gas, solvent, and waste utilities. Fixed costs include labor, equipment maintenance, and capital depreciation. Feedstock could have a great influence on the MFSP. In this analysis, the feedstock cost is assumed to be \$66 dry tonne $^{-1}$ [9]. Prices of natural gas and electricity (\$5.59 GJ^{-1} and \$79 MWh^{-1}) are obtained from the Energy Information Administration (EIA) database [40]. Prices of other raw materials are obtained from previously published literature [9, 41-43].

3.1 Sensitivity analysis

Some process parameters might vary during operation of the SL plant and facility. Therefore, a sensitivity analysis is employed to evaluate any impact of parameter changes on the MSFP. In this analysis, the parameters considered are product fuel yield, fixed capital investment, IRR, feedstock cost, income tax rate, working capital, and hydrotreating cost. Sensitivity analysis is conducted by assuming some key range process parameters. A fairly large range is taken into account for a potential variation on the feedstock price. The range

employed is (-50% to 100%). For all other parameters, a ±20% range is used. MFSP is estimated for the base case, the high-end, and the low-end values for each parameter.

The sensitivity analysis is conducted by evaluating the MSFP after changing one parameter, while the rest remain fixed. This approach is necessary for giving a clear understanding of the impact of each individual parameter. In practice, several parameter values would vary simultaneously but a multivariate sensitivity analysis is not evaluated in this study.

4. Results and discussion

4.1 Mass and energy balances

The process model estimates that a 2000 dry tonne feedstock per day plant produces 439 dam^3 of liquid fuel per day, for which 364 dam^3 of MWO and 76 dam^3 of HWO. These results translate to a fuel yield of 0.691 dam^3 dry $tonne^{-1}$ feedstock. The simulation also provides estimates for utility usage. Cooling make-up water and boiler feed water are the major uses of water in the plant, totaling 23.3 tonne h^{-1}. Process off-gases are combusted to provide process heat with excess heat used for superheated steam generation. Most of the process heat is consumed by the SL reactor [43-47]. Generated steam is mainly used for two different purposes, which includes heating source in the process and electricity generation. Even though electricity is being produced in the steam plant, the process is not self-sufficient in electricity. Therefore, the facility imports electricity. The largest portion of the electricity is used for SL since pumping Pinewood into the reactor requires a great amount of energy. Table 6 shows a summary of the process modeling results.

Table 6: Summary of process modeling results

PineMarwood rate (dry tonne day^{-1})	2000
Overall process yields	
MWO (dam^3 $year^{-1}$)	364
HWO (dam^3 $year^{-1}$)	76
Water usage	
Boiler feed water (tonne day^{-1})	323
Cooling water makeup (tonne day^{-1})	730
Electricity usage	
Electricity required (MW)	9.1
Electricity generated (MW)	3.0
Purchased electricity (MW)	6.1

4.2 Cost analysis

Major economic results are shown in Table 6 and 7. The MFSP of both MWO (MWO) and HWO is estimated to be $ 0.94/gallon. The 2000 dry tonne day^{-1} plant requires a TPEC of $65 M and a TIC of $196 M. The major contributor to this cost is the SL plant, accounting for 62% of the fixed capital cost, which is mainly due to the higher cost of pressure vessels for the SL reactor. Steam generation accounts for 25% of the capital cost. The flow separation accounts for 13%. SL is still in an early development stage, and the technology employed in future plant construction could require a significantly different capital investment than estimated in this analysis. The FCI was varied in the sensitivity analysis to better estimate any potential risk and impacts on the MFSP.

Table 7: Economic analysis results (all results in 2011 dollars)

Total purchased equipment cost (TPEC)	100% TPEC	65M$
Direct installed cost (DIC)	302% TPEC	196M$
Indirect installed cost (TIC)	126% TPEC	82M$
Fixed capital investment (FCI)	428% TPEC	282M$
Working capital	15% TPEC	50M$
Land	6% TPEC	6M$
Total project investment (TPI)	510% TPEC	331M$

The total annual operating costs are evaluated at $110 M, and the feedstock accounts for 37% of operating cost, followed by fixed costs (14%) and capital depreciation (12%). Electricity and other utilities account for 3% of the annual operating costs. The operating cost constitutes 56% of the cost while the capital cost constitutes about 44%. SL constitutes about 33% of the conversion cost. Different areas of contributions to operating costs are shown in Figure 3. This result is in agreement with the high capital cost of the SL reactor. Bio-crude upgrading and refining also contribute to more than 21% of conversion cost.

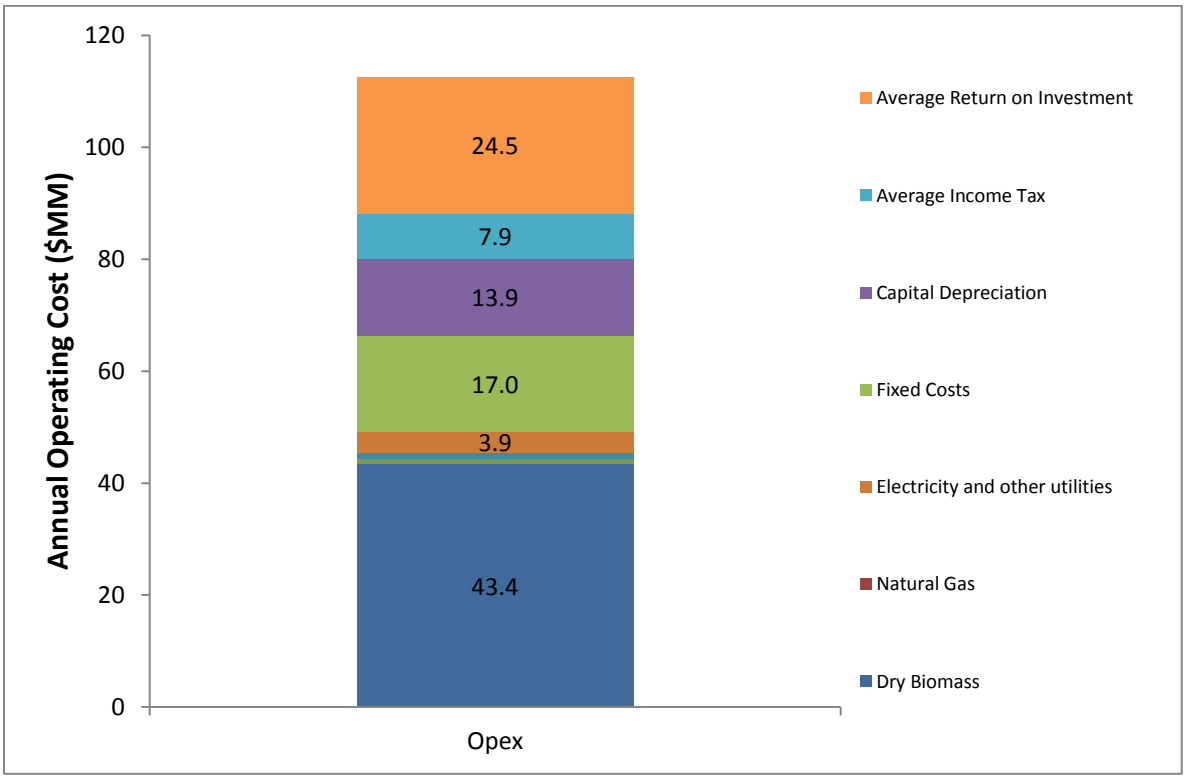

Figure 3: Annual operating cost for producing MWO and HWO from pinewood with hydrocarbon solvent via SL

Table 8: Major economic analysis results (all results are in 2011 dollars)

M$	
Fixed capital investment	
Solvent liquefaction	209
Steam generation	66
Fractionation	45
Auxiliaries	23
Total fixed capital investment	343
Annual operating cost	
Feedstock	43.4
Natural gas	6.7
Waste disposal	4.1
Electricity and other utilities	3.9
Fixed costs	17
Average income tax	8
Average return on investment	25.6
Total annual operating cost	110
MFSP, $/gallon	0.94

4.3 Sensitivity analysis results

Results of the sensitivity analysis are shown in Figure 4. The results obtained are based on ±20% changes to the parameter values except for the feedstock cost for which a larger range (-50% to +100%) is used to account for its price uncertainty. Figure 4 illustrates that product yields and feedstock cost have the greatest impact on MFSP. The ± 20% variation in fuel yields result in a MSFP range of $0.80/gallon to $1.19/gallon. Different factors could impact the final product yield, including bio-crude yield and separation efficiencies. In this analysis, the yield of hydroprocessing is calculated based on experimental data rather than assumptions. The results obtained from the sensitivity analysis showed the necessity of conducting further experiments to better understand the yields of bio-crude production [48-55].

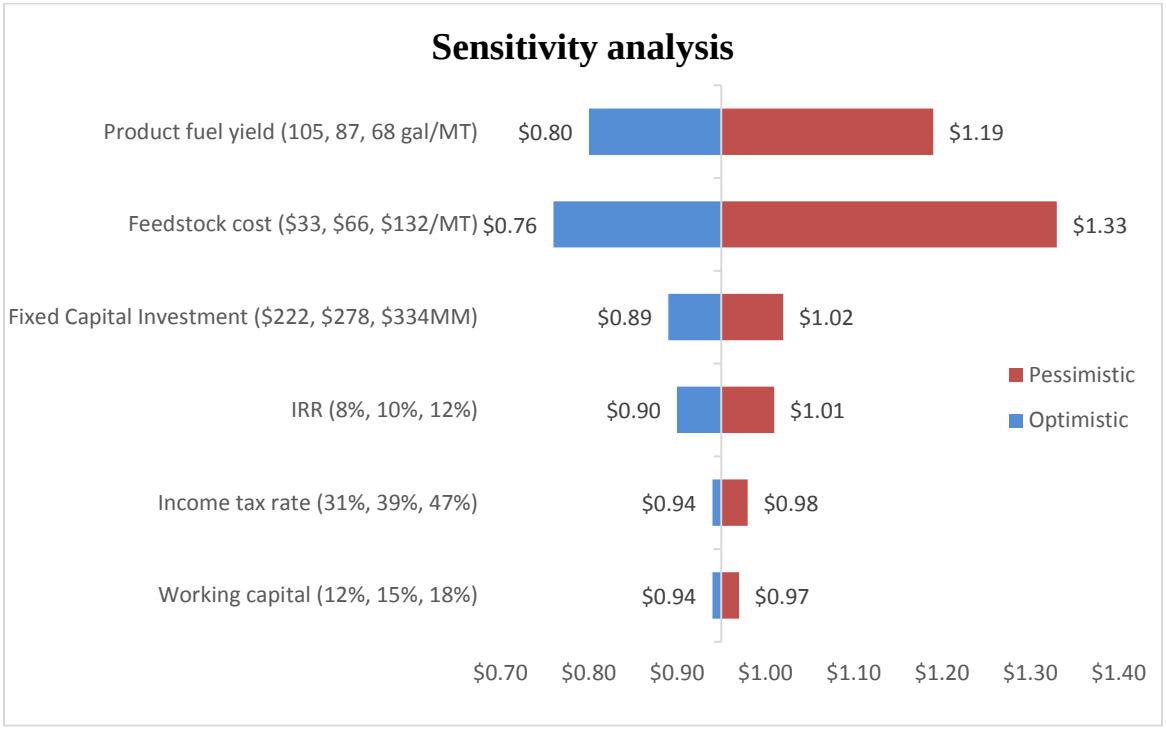

Figure 4: Sensitivity analysis of the minimum fuel selling price to select technical and economic parameters.

Pinewood prices could vary significantly based on availability and demand. If the feedstock can be purchased at a cost of \$33 dry tonne^{-1}, the sensitivity analysis demonstrates that the MFSP can be as low as \$0.80/gallon. On the other hand, if the feedstock was purchased at \$132 dry tonne^{-1}, the MFSP would increase to \$1.19/gallon. The next sensitive parameters in terms of impact to the MSFP are the fixed capital investment and IRR. A 20% increase in fixed capital investment and IRR will result in 8% and 7% increase in MFSP respectively.

5. Conclusions

This techno-economic analysis investigated the minimum fuel selling price for medium wood oil and heavy wood oil fuels from SL of pinewood based on an experimental study conducted on a pilot scale. It is concluded that SL of pinewood for future upgrading to bio-oil is a promising pathway for the production of biofuels. The minimum fuel selling price for medium wood oil and heavy wood oil produced from SL is economically viable and competitive with petroleum-derived transportation fuels. The sensitivity analysis demonstrated that the MFSP is the most sensitive to product fuel yield. Parameters like fixed capital investment, IRR, and feedstock also have great influence on the MFSP.

References

[1] S. Thangalazhy-Gopakumar, S. Adhikari, H. Ravindran, R. B. Gupta, O. Fasina, M. Tu, and S. D. Fernando, "Physiochemical properties of bio-oil produced at various temperatures from pine wood using an auger reactor," *Bioresource. Technol.*, vol. 101, no. 21, pp. 8389–8395, 2010.

[2] G. Yildiz, F. Ronsse, R. Venderbosch, R. van Duren, S. R. A. Kersten, and W. Prins, "Effect of biomass ash in catalytic fast pyrolysis of pine wood," *Appl. Catalytic. B Environ.* Vol. 168–169, pp. 203–211, 2015.

[3] F. Antony, L. R. Schimleck, R. F. Daniels, A. C. Iii, B. E. Borders, M. B. Kane, and H. E. Burkhart, "Whole-Tree Bark and Wood Properties of Loblolly Pine from Intensively Managed Plantations," vol. 61, no. February, pp. 55–66, 2015.

[4] A. Ferraz, J. Baeza, J. Rodriguez, and J. Freer, "Estimating the chemical composition of biodegraded pine and eucalyptus wood by DRIFT spectroscopy and multivariate analysis," *Bioresource. Technol.*, vol. 74, no. 3, pp. 201–212, 2000.

[5] B. R. T. Simoneit, W. F. Rogge, Q. Lang, and R. Jaffé, "Molecular characterization of smoke from campfire burning of pine wood (Pinus Elliott)," *Chemosph. - Glob. Chang. Sci.*, vol. 2, no. 1, pp. 107–122, 2000.

[6] D. Mohan, C. U. Pittman, M. Bricka, F. Smith, B. Yancey, J. Mohammad, P. H. Steele, M. F. Alexandre-Franco, V. Gómez-Serrano, and H. Gong, "Sorption of arsenic, cadmium, and lead by chars produced from fast pyrolysis of wood and bark during bio-oil production," *J. Colloid Interface Sci.*, vol. 310, no. 1, pp. 57–73, 2007.

[7] Q. Sun, S. Yu, F. Wang, and J. Wang, “Decomposition and gasification of pyrolysis volatiles from pine wood through a bed of hot char,” *Fuel*, vol. 90, no. 3, pp. 1041–1048, 2011.

[8] Y. Zhu, M. J. Biddy, S. B. Jones, D. C. Elliott, and A. J. Schmidt, “Techno-economic analysis of liquid fuel production from woody biomass via solvent liquefaction(SL) and upgrading,” *Appl. Energy*, vol. 129, pp. 384–394, 2014.

[9] R. C. Taylor C. Schulz, Martin R, Haverly, Lysle E. Whitmer, Andrew J. Friend, Jordan Funkhouser, Ryan G.Smith, and Brown, “Continuous Pilot-Scale Loblolly Pine Liquefaction to a Partially Deoxygenated Bio-Oil,” Ames, IA, 2016.

[10] Z. Liu, F. S. Zhang, and J. Wu, “Characterization and application of chars produced from pinewood pyrolysis and hydrothermal treatment,” *Fuel*, vol. 89, no. 2, pp. 510–514, 2010.

[11] A. V. Bridgewater, “Review of fast pyrolysis of biomass and product upgrading,” *Biomass and Bioenergy*, vol. 38. pp. 68–94, 2012.

[12] M. Bertero, G. De La Puente, and U. Sedran, “Fuels from bio-oils: Bio-oil production from different residual sources, characterization and thermal conditioning,” *Fuel*, vol. 95, pp. 263–271, 2012.

[13] A. Oasmaa, Y. Solantausta, V. Arpiainen, E. Kuoppala, and K. Sipilä, “Fast pyrolysis bio-oils from wood and agricultural residues,” *Energy and Fuels*, vol. 24, no. 2, pp. 1380–1388, 2010.

[14] W. Zhang, J. Chen, R. Liu, S. Wang, L. Chen, and K. Li, “Hydrodeoxygenation of Lignin-Derived Phenolic Monomers and Dimers to Alkane Fuels over Bifunctional Zeolite-Supported Metal Catalysts,” 2014.

[15] G. W. Huber, S. Iborra, and A. Corma, “Synthesis of Transportation Fuels from Biomass : Chemistry, Catalysts, and Engineering,” vol. 2, pp. 4044–4098, 2006.

[16] J. Zakzeski, P. C. A. Bruijnincx, A. L. Jongerius, and B. M. Weckhuysen, “The Catalytic Valorization of Lignin for the Production of Renewable Chemicals,” pp. 3552–3599, 2010.

[17] S. Crossley, J. Faria, M. Shen, and D. E. Resasco, “Solid Nanoparticles that Catalyze Biofuel Upgrade Reactions at the Water / Oil Interface,” *Science (80-.).*, vol. 327, no. December, pp. 68–72, 2009.

[18] Peterson AA, Vogel F, Lachance RP, Froling M, Antal JMJ, Tester JW. Thermochemical biofuel production in hydrothermal media: a review of sub- and supercritical water technologies. Energy Environ Sci 2008; 1(1):32e65

[19] J. Akhtar and N. A. S. Amin, “A review on process conditions for optimum bio-oil yield in solvent liquefaction of biomass,” *Renewable and Sustainable Energy Reviews*, vol. 15, no. 3. pp. 1615–1624, 2011.

[20] L. Ou, R. Thilakaratne, R. C. Brown, and M. M. Wright, “Techno-economic analysis of transportation fuels from defatted microalgae via solvent liquefaction and hydroprocessing,” *Biomass and Bioenergy*, vol. 72, pp. 45–54, 2015.

[21] D. Maldas and N. Shiraishi, “Liquefaction of biomass in the presence of phenol and H2O using alkalies and salts as the catalyst,” *Biomass and Bioenergy*, vol. 12, no. 4, pp. 273–279, 1997.

[22] D. Meier, D. R. Larimer, and O. Faix, “Direct liquefaction of different lignocellulosics and their constituents. 1. Fractionation, elemental composition,” *Fuel*, vol. 65, no. 7, pp. 910–915, 1986.

[23] H. H. Markus Bolhàr-Nordenkampf, “Gasification demonstration plants in chip-biomass gasification plant güssing,” *Dimens. Contemp. Ger. Arts Lett.* vol. 2, no. 1, pp. 227–230, 2004.

[24] I. A. Vasalos, A. A. Lappas, E. P. Kopalidou, and K. G. Kalogiannis, “Biomass catalytic pyrolysis: Process design and economic analysis,” *Wiley Interdisciplinary Reviews: Energy and Environment*, vol. 5, no. 3. pp. 370–383, 2016.

[25] S. Jones, Y. Zhu, D. Anderson, R. T. Hallen, and D. C. Elliott, “Process Design and Economics for the Conversion of Algal Biomass to Hydrocarbons : Whole Algae Solvent liquefaction and Upgrading,” no. March, p. 69, 2014.

[26] D. Humbird, R. Davis, L. Tao, C. Kinchin, D. Hsu, A. Aden, P. Schoen, J. Lukas, B. Olthof, M. Worley, D. Sexton, and D. Dudgeon, “Process Design and Economics for Biochemical Conversion of Lignocellulosic Biomass to Ethanol,” *Renew. Energy*, vol. 303, no. May, p. 147, 2011.

[27] S. Jones, C. Valkenburg, and C. Walton, “Production of Gasoline and Diesel from Biomass via Fast Pyrolysis, Hydrotreating and Hydrocracking: a design case,” *Energy*, no. February, p. 76, 2009.

[28] F. K. Kazi, J. Fortman, and R. Anex, “Techno-Economic Analysis of Biochemical Scenarios for Production of Cellulosic Ethanol,” *Natl. Renew. Energy Lab.*, no. June, p. 102, 2010.

[29] Meyers RA. Handbook of petroleum refining processes. 3rd Ed. New York: McGraw-Hill; 2004.

[30] Aspen Technology, Inc., Aspen plus 2006.5 user manual. Cambridge, Massachusetts; 2007.

[31] M. S. Noori and K. Karimi, “Chemical and structural analysis of alkali pretreated pinewood for efficient ethanol production,” *RSC Adv.*, vol. 6, no. 70, pp. 65683–65690, 2016.

[32] Turton R, Bailie RC, Whiting WB, Shaeiwitz JA. Analysis, synthesis and design of chemical processes. 3rd ed. Boston: Pearson Education; 2008.

[33] R. D. Perlack, B. J. Stokes, L. M. Eaton, and A. F. Turnhollow, “US Billion-ton update. Biomass Supply for a Bioenergy and Bioproducts Industry,” *Renewable. Energy*, vol. 7, no. August, pp. 1–229, 2005.

[34] R. M. Swanson, J. a Satrio, R. C. Brown, and D. D. Hsu, “Techno-Economic Analysis of Biofuels Production Based on Gasification Techno-Economic Analysis of Biofuels Production Based on Gasification Alexandru Platon,” *Energy*, vol. 89, no. November, pp. S11–S19, 2010.

[35] Peters MS, Timmerhaus KD, West RE. Plant design and economics for chemical engineers. 5th Ed. New York: McGraw-Hill; 2003.

[36] R. Thilakaratne, T. Brown, Y. Li, G. Hu, and R. Brown, “Mild catalytic pyrolysis of biomass for production of transportation fuels: a techno-economic analysis,” *Green Chemistry*, vol. 16, no. 2. p. 627, 2014.

[37] SRI. PEP yearbook international 2007. Menlo Park (CA): SRI International; 2007

[38] EIA. Electric power monthly with data for April 2013. Independent statistics & analysis. Washington (DC): U.S. Energy Information Administration; 2013.

[39] Elliott DC, Hart TR, Schmidt AJ, Neuenschwander GG, Rotness LJ, Olarte MV, et al. Process development for solvent liquefaction of algae feedstocks in a continuous-flow reactor. Algal Res 2013; 2(4):445e54.

[40] Skone TJ. Role of alternative energy sources: natural gas technology assessment. Pittsburgh (PA): National Energy Technology Laboratory; 2012. Report no.: DOE/NETL-2012/1539. Contract no.: DE-FE0004001. Sponsored by the Department of Energy.

[41] EIA. Electric power monthly with data for April 2013. Independent statistics & analysis. Washington (DC): U.S.Energy Information Administration; 2013.

[42] EIA. Annual energy outlook 2011. Independent statistics & analysis. Report no.: DOE/EIA-0383. Washington (DC): U.S. Energy Information Administration; 2011.

[43] Haynes HW, Parcher JF, Helmer NE. Hydrocracking polycyclic hydrocarbons over a dual-functional zeolite (faujasite)-based catalyst. Ind Eng Chem Process Des Dev (Ind Eng Chem Res) 1983; 22:401–9.

[44] B. A. Black, W. E. Michener, K. J. Ramirez, M. J. Biddy, B. C. Knott, M. W. Jarvis, J. Olstad, O. D. Mante, D. C. Dayton, and G. T. Beckham, "Aqueous Stream Characterization from Biomass Fast Pyrolysis and Catalytic Fast Pyrolysis," 2016.

[45] Z. Zhu, L. Rosendahl, S. S. Toor, D. Yu, and G. Chen, "Solvent liquefaction of barley straw to bio-crude oil: Effects of reaction temperature and aqueous phase recirculation," *Appl. Energy*, vol. 137, pp. 183–192, 2015.

[46] L. Snowden-Swan, Y. Zhu, S. Jones, D. Elliott, A. Schmidt, R. Hallen, J. Billing, T. Hart, S. Fox, and G. Maupin, "Solvent liquefaction and Upgrading of Municipal Wastewater Treatment Plant Sludge: A Preliminary Techno-Economic Analysis," p. PNNL-25464, 2016.

[47] T. M. Brown, P. Duan, and P. E. Savage, "Solvent liquefaction and gasification of Nannochloropsis sp.," *Energy and Fuels*, vol. 24, no. 6, pp. 3639–3646, 2010.

[48] D. C. Elliott, P. Biller, A. B. Ross, A. J. Schmidt, and S. B. Jones, "Solvent liquefaction of biomass: Developments from batch to continuous process," *Bioresource. Technol.*, vol. 178, pp. 147–156, 2015.

[49] Y. Wang, H. Wang, H. Lin, Y. Zheng, J. Zhao, A. Pelletier, and K. Li, "Effects of solvents and catalysts in liquefaction of pinewood sawdust for the production of bio-oils," *Biomass and Bioenergy*, vol. 59, pp. 158–167, 2013.

[50] J. C. Quinn and R. Davis, "The potentials and challenges of algae based biofuels: A review of the techno-economic, life cycle, and resource assessment modeling," *Bioresource. Technol.*, vol. 184, pp. 444–452, 2015.

[51] A. J. Ragauskas, M. Nagy, D. H. Kim, C. a. Eckert, J. P. Hallett, and C. L. Liotta, "From wood to fuels: Integrating biofuels and pulp production," *Ind. Biotechnology.*, vol. 2, no. 1, pp. 55–65, 2006.

[52] E. Panisko, T. Wietsma, T. Lemmon, K. Albrecht, and D. Howe, "Characterization of the aqueous fractions from hydrotreatment and solvent liquefaction of lignocellulosic feedstocks," *Biomass and Bioenergy*, vol. 74, no. March, pp. 162–171, 2015.

[53] E. R. Venteris, R. L. Skaggs, M. S. Wigmosta, and A. M. Coleman, "A national-scale comparison of resource and nutrient demands for algae-based biofuel production by lipid extraction and hydrothermal liquefaction," *Biomass and Bioenergy*, vol. 64, pp. 276–290, 2014.

[54] Y. Zhu, K. O. Albrecht, D. C. Elliott, R. T. Hallen, and S. B. Jones, "Development of solvent liquefaction and upgrading technologies for lipid-extracted algae conversion to liquid fuels," *Algal Res.*, vol. 2, no. 4, pp. 455–464, 2013.

[55] E. D. Frank, A. Elgowainy, J. Han, and Z. Wang, “Life cycle comparison of solvent liquefaction and lipid extraction pathways to renewable diesel from algae,” *Mitig. Adapt. Strategy. Glob. Chang.* vol. 18, no. 1, pp. 137–158, 2013.de

CHAPTER 4. GENERAL CONCLUSION

Cavitation phenomena were investigated in both ball and butterfly valves using the commercial software ANSYS FLUENT. This study evaluated the possibility of reducing vapor volume fraction (cavitation) in both valves by respectively setting design constraint for each one. The major design parameters were determined, a design of experiments provided a response surface, which was optimized for an optimal design. An adaptive multiple-objective design was used in FLUENT to determine the optimal design. The best candidate for the optimal design of each valve was found although they did not meet all the constraints set by the designer. This study is a good foundation and a promising route for producing an optimal design to reduce cavitation using computational fluid dynamics techniques.

The techno-economic analysis of solvent liquefaction of pinewood for medium wood and heavy wood oil fuels was investigated. The minimum fuel selling price was estimated for both medium wood oil and heavy wood oil; different parameters influencing the fuel price such as product fuel yield, feedstock, fixed capital investment, and internal rate of return were examined. Solvent liquefaction of pinewood for future upgrade to bio-oil is could be a promising pathway to produce biofuels. The minimum fuel selling price for medium oil and heavy wood oil produced via solvent liquefaction is economically viable and competitive with petroleum-derived transportation fuels.